



## Smooth Tight Frame Wavelets and Image Microanalysis in the Fourier Domain\*

R. ASHINO

Division of Mathematical Sciences, Osaka Kyoiku University  
Kashiwara, Osaka 582-8582, Japan  
ashino@cc.osaka-kyoiku.ac.jp

S. J. DESJARDINS

Department of Mathematics and Statistics, University of Ottawa  
Ottawa, Ontario, Canada K1N 6N5  
desjards@mathstat.uottawa.ca

C. HEIL

School of Mathematics, Georgia Institute of Technology  
Atlanta, GA 30332, U.S.A.  
heil@math.gatech.edu

M. NAGASE

Department of Mathematics, Osaka University  
Toyonaka, Osaka 560-0043, Japan  
nagase@math.wani.osaka-u.ac.jp

R. VAILLANCOURT

Department of Mathematics and Statistics, University of Ottawa  
Ottawa, Ontario, Canada K1N 6N5  
remi@uottawa.ca

*(Received and accepted June 2002)*

**Abstract**—General results on microlocal analysis and tight frames in  $\mathbb{R}^2$  are summarized. To perform microlocal analysis of tempered distributions, orthogonal multiwavelets, whose Fourier transforms consist of characteristic functions of squares or sectors of annuli, are constructed in the Fourier domain and are shown to satisfy a multiresolution analysis with several choices of scaling functions. To have good localization in both the  $x$  and Fourier domains, redundant smooth tight wavelet frames, with frame bounds equal to one, called Parseval wavelet frames, are obtained in the Fourier domain by properly tapering the above characteristic functions. These nonorthogonal frame wavelets can be generated by two-scale equations from a multiresolution analysis. A natural formulation of the problem is by means of pseudodifferential operators. Singularities, which are added to smooth images, can be localized in position and direction by means of the frame coefficients of the filtered images computed in the Fourier domain. Using Plancherel's theorem, the frame expansion of the filtered images is obtained in the  $x$  domain. Subtracting this expansion from the scarred images restores the original images. © 2003 Elsevier Science Ltd. All rights reserved.

\*Dedicated to Professor Atsushi Yoshikawa on the occasion of his 60<sup>th</sup> birthday.

This research was partially supported by the Japanese Ministry of Education, Culture, Sports, Science and Technology, Grant-in-Aid for Scientific Research (C), 11640166(2000), 13640171(2001–2002), NSF Grant DMS-9970524, and NSERC of Canada.

**Keywords**—Smooth tight frame, Microlocal analysis, Localization of singularity.

## 1. INTRODUCTION

The concept of frames for Hilbert spaces generalizes the notion of orthonormal and Riesz bases in the sense that a frame  $X = \{x_i; i \in I\}$ , where  $I$  is an index set, provides a stable representation for signals  $f$  by means of an expansion  $f = \sum_i c_i(f)x_i$ . However,  $X$  need not be an orthonormal or independent sequence. Frames are useful for signal decomposition in cases where redundancy, robustness, oversampling, and irregular sampling play a role (see [1,2]).

Nonsmooth orthonormal multiwavelets have been constructed in [3] for performing microlocal analysis of tempered distributions in  $\mathbb{R}^n$ . The multiwavelets, whose Fourier transforms consist of characteristic functions of cubes, have perfect localization in the Fourier domain but poor localization in the  $x$  domain. To obtain good localization in both the  $x$  and Fourier domains in  $\mathbb{R}^n$ , in [4], the block wavelets are smoothed by convolution and normalized to produce tight frames with frame bounds equal to one, called Parseval frames. In [5], nonorthogonal rectangular and polar smooth frame wavelets in  $\mathbb{R}^2$  are obtained from a multiresolution analysis.

In [6], on the one hand, it is shown that no smooth orthonormal wavelets exist in the Hardy space  $H^2(\mathbb{R})$  of  $L^2$  functions whose Fourier transforms have support on the positive real axis, but, on the other hand, smooth frame wavelets for  $H^2(\mathbb{R})$  are constructed with good localization in both the  $x$  and Fourier domains.

In the present paper, attention is restricted to microlocal analysis in the two-dimensional case with the goal of localizing the singularities of a function  $f$  in the time domain by analyzing the growth of  $\hat{f}$  in wedges in the Fourier domain.

Since wedges in  $\mathbb{R}^2$  are generalizations of the positive real axis in  $\mathbb{R}$ , smooth frame wavelets are generalized to  $L^2(\mathbb{R}^2)$  by properly tapering the Fourier transforms of the orthonormal multiwavelets given in [3]. Thus, the dyadically scaled Fourier transforms of the twelve frame wavelets

$$\{\psi^1(x), \psi^2(x), \dots, \psi^{12}(x)\}$$

satisfy the identity

$$G(\xi) := \sum_{\substack{\ell=1,2,\dots,12 \\ j \in \mathbb{Z}}} \left| \hat{\psi}^\ell(2^j \xi) \right|^2 \equiv 1, \quad \xi \neq 0. \quad (1)$$

In a multiresolution analysis, the shifted and scaled scaling function  $\phi_{j,k}(x) = 2^j \phi(2^j x - k)$  are orthonormal bases of subspaces  $V_j$ . Although our smooth frame wavelets can be derived from a multiresolution analysis by two-scale equations, they are not orthogonal to each other, nor to the spaces  $V_j$ .

The paper proceeds as follows. In Section 2, continuous and discrete Fourier transforms of line impulses are described. In Section 3, the concepts of microlocal analysis are reviewed. In Section 4, necessary and sufficient conditions are given to characterize tight frame wavelets. In Section 5, different pavings of the Fourier domain for microlocal analysis are presented. In Section 6, a multiresolution analysis is presented for wavelets with box Fourier transforms. Section 7 presents painless smooth tight frame wavelets. Section 8 is concerned with rings of 12 tapered frame wavelets. Section 9 presents a multiresolution analysis for smooth rectangular frame wavelets. Section 10 describes a general construction of microlocal frame wavelets. Section 11 introduces a multiresolution analysis for smooth polar frames wavelets. Section 12 contains a numerical implementation of the localization method applied to geometric and natural images.

The above methods fall within the concept of pseudodifferential operators, and this work could alternatively be considered within the context of almost orthogonal decompositions by means of  $\phi$ -transforms as presented, for instance, in [7,8].

## 2. FOURIER TRANSFORM OF LINE IMPULSES

In view of numerical applications on domains with pixels at integer points, the continuous Fourier transform  $\hat{f}(\xi)$  of a function  $f(x)$  defined over  $\mathbb{R}^2$  and the inverse Fourier transform of  $\hat{f}(\xi)$  will be

$$\mathcal{F}f(\xi) := \hat{f}(\xi) = \int e^{-2\pi i \xi \cdot x} f(x) dx, \quad \mathcal{F}^{-1}f(x) := f(x) = \int e^{2\pi i x \cdot \xi} \hat{f}(\xi) d\xi, \quad (2)$$

and Plancherel's theorem will be

$$\langle f, g \rangle = \langle \hat{f}, \hat{g} \rangle, \quad (3)$$

where

$$\langle f, g \rangle = \int_{\mathbb{R}^2} f(x) \overline{g(x)} dx, \quad \langle \hat{f}, \hat{g} \rangle = \int_{\mathbb{R}^2} \hat{f}(\xi) \overline{\hat{g}(\xi)} d\xi.$$

A fundamental result that is used in this work is concerned with the Fourier transform of parallel straight lines and parallel straight segments. The continuous Fourier transform of a line impulse distribution in  $\mathbb{R}^2$  is a line impulse distribution at right angles to the original line impulse distribution. It is enough to show this result for a line impulse along the  $x_1$ -axis.

**PROPOSITION 1.** *Let the tensor product of the identity function  $1_{x_1}$  and the Dirac measure  $\delta(x_2)$ ,*

$$f(x_1, x_2) = 1_{x_1} \otimes \delta(x_2),$$

*be a line impulse distribution along the  $x_1$ -axis. Then the Fourier transform*

$$\hat{f}(\xi_1, \xi_2) = \delta(\xi_1) \otimes 1_{\xi_2}$$

*is a line impulse distribution along the  $\xi_2$ -axis. The Fourier transforms of parallel line impulse distributions differ by the phase of their elements.*

**PROOF.** For  $t$  and  $\omega \in \mathbb{R}$ , we have  $\hat{1}_t(\omega) = \delta(\omega)$  and  $\hat{\delta}(t) = 1_t$ . Hence, by the definition of the tensor product of distributions, the Fourier transform acts separately on each component; thus, we have

$$\hat{f}(\xi_1, \xi_2) = \left( \hat{1}_{x_1} \otimes \hat{\delta}(x_2) \right) (\xi_1, \xi_2) = \delta(\xi_1) \otimes 1_{\xi_2}.$$

Let  $f(x_1, x_2)$  be a line impulse distribution along the line  $x_2 = r$ ; that is,

$$f(x_1, x_2) = 1_{x_1} \otimes \delta(x_2 - r).$$

Since  $\widehat{\delta(t-r)}(\omega) = e^{-2\pi i r \omega} 1_\omega$ , where  $t, r, \omega \in \mathbb{R}$ , we have

$$\hat{f}(\xi_1, \xi_2) = \left( \hat{1}_{x_1} \otimes \widehat{\delta(x_2 - r)} \right) (\xi_1, \xi_2) = \delta(\xi_1) \otimes e^{-2\pi i r \xi_2} 1_{\xi_2}. \quad \blacksquare$$

The discrete Fourier transform  $X(k_1, k_2)$  of a sequence  $x(n_1, n_2)$  and the inverse discrete Fourier transform of  $X(k_1, k_2)$  are

$$X(k_1, k_2) = \sum_{n_2=1}^N \sum_{n_1=1}^N x(n_1, n_2) e^{-2\pi i (k_1-1)(n_1-1)/N} e^{-2\pi i (k_2-1)(n_2-1)/N} \quad (4)$$

and

$$x(n_1, n_2) = \frac{1}{N^2} \sum_{k_2=1}^N \sum_{k_1=1}^N X(k_1, k_2) e^{2\pi i (k_1-1)(n_1-1)/N} e^{2\pi i (k_2-1)(n_2-1)/N}. \quad (5)$$

A result similar to Proposition 1 holds for the discrete Fourier transform of a line impulse. Hereafter, we use the MATLAB colon ( $:$ ) convention; that is,  $1 : N$  means  $1, 2, \dots, N$ .

PROPOSITION 2. *Let*

$$x(n_1, n_2) = \begin{cases} 1, & n_1 = 1, \quad n_2 = 1 : N, \\ 0, & \text{otherwise,} \end{cases}$$

*be a line impulse along the first row of an  $N \times N$  matrix. Then the discrete Fourier transform*

$$X(k_1, k_2) = \begin{cases} 1, & k_1 = 1 : N, \quad k_2 = 1, \\ 0, & \text{otherwise,} \end{cases}$$

*is a line impulse along the first column of the matrix. The Fourier transforms of parallel line impulses differ by the phase of their elements.*

PROOF. A simple summation gives

$$\begin{aligned} X(k_1, k_2) &= \sum_{n_2=1}^N \sum_{n_1=1}^N x(n_1, n_2) e^{-2\pi i(k_1-1)(n_1-1)/N} e^{-2\pi i(k_2-1)(n_2-1)/N} \\ &= \sum_{n_2=1}^N e^{-2\pi i(k_2-1)(n_2-1)/N} \\ &= \begin{cases} N, & k_1 = 1 : N, \quad k_2 = 1, \\ 0, & \text{otherwise.} \end{cases} \end{aligned}$$

Let  $x(n_1, n_2)$  be a line impulse along the  $r^{\text{th}}$  row. Then

$$\begin{aligned} X(k_1, k_2) &= \sum_{n_2=1}^N \sum_{n_1=1}^N x(n_1, n_2) e^{-2\pi i(k_1-1)(n_1-1)/N} e^{-2\pi i(k_2-1)(n_2-1)/N} \\ &= e^{-2\pi i(k_1-1)(r-1)/N} \sum_{n_2=1}^N e^{-2\pi i(k_2-1)(n_2-1)/N} \\ &= \begin{cases} N e^{-2\pi i(k_1-1)(r-1)/N}, & k_1 = 1 : N, \quad k_2 = 1, \\ 0, & \text{otherwise,} \end{cases} \end{aligned}$$

which is a modulated line impulse in the vertical direction. ■

The discrete Fourier transform of a constant segment along a row of a matrix produces an approximation to the cardinal sine in the  $k_2$ -variable which is modulated in the  $k_1$ -variable, as a simple computation shows.

Let

$$x(n_1, n_2) = \begin{cases} 1, & n_1 = r_1, \quad n_2 = r_2 : r_3, \\ 0, & \text{otherwise,} \end{cases}$$

be a segment impulse along the  $r_1^{\text{th}}$  row of an  $N \times N$  matrix. Then the discrete Fourier transform of  $x$  is

$$\begin{aligned} X(k_1, k_2) &= \sum_{n_2=1}^N \sum_{n_1=1}^N x(n_1, n_2) e^{-2\pi i(k_1-1)(n_1-1)/N} e^{-2\pi i(k_2-1)(n_2-1)/N} \\ &= e^{-2\pi i(k_1-1)(r_1-1)/N} \left[ \sum_{n_2=r_2}^{r_3} e^{-2\pi i(k_2-1)(n_2-1)/N} \right], \end{aligned}$$

where the term in square brackets is an approximation to the cardinal sine. By means of the MATLAB `fftshift` command, the vertical peak line of  $X(k_1, k_2)$  passes through the center of the matrix. The larger that  $N$  becomes and the longer the segment becomes, the closer the surface will be to a modulated line impulse.

### 3. MICROLOCAL ANALYSIS

Our smooth tight frame wavelets are intended to be used for investigating the microanalytic content of distributions. To motivate such constructions, in this section we summarize the expositions found in [3,4,9].

Intuitively, hyperfunctions, which were introduced by Sato [10] and extensively developed by the Kyoto school of mathematics, can be considered as sums of boundary values of holomorphic functions defined in infinitesimal wedges. Hyperfunctions are powerful tools in several applications: for example, vortex sheets in two-dimensional fluid dynamics are a realization of one-dimensional hyperfunctions. Analytic continuation in domains of special forms plays a key role in the theory of hyperfunctions. A simple example of a hyperfunction is the Dirac delta measure  $\delta(x)$ , which, when applied to a continuous function  $f(x)$  produces the value  $f(0)$

$$\langle f, \delta \rangle = \int_{\mathbb{R}} f(x) \delta(x) dx = f(0).$$

Since, in Schwartz's theory of distributions [11], smooth testing functions of compact support cannot be holomorphic functions, Sato used Cauchy's integral formula to define  $\delta(x)$  applied to a holomorphic function  $f(z)$  on an open set  $D \subset \mathbb{C}$ . Assuming that  $0 \in D$  and letting  $\gamma = \partial D$  denote the boundary of  $D$ , we have

$$\frac{1}{2\pi i} \oint_{\gamma} \frac{f(z)}{z} dz = f(0).$$

In the limit as the path  $\gamma$  is shifted to  $\gamma_+ + \gamma_-$ , where  $\gamma_+$  goes from  $+\infty$  to  $-\infty$  and  $\gamma_-$  goes from  $-\infty$  to  $+\infty$  along the real axis, as shown in Figure 1, this formula becomes

$$\frac{1}{2\pi i} \oint_{\gamma} \frac{f(z)}{z} dz = \int_{-\infty}^{+\infty} \left( -\frac{1}{2\pi i} \right) \left( \frac{1}{x+i0} - \frac{1}{x-i0} \right) f(x) dx.$$

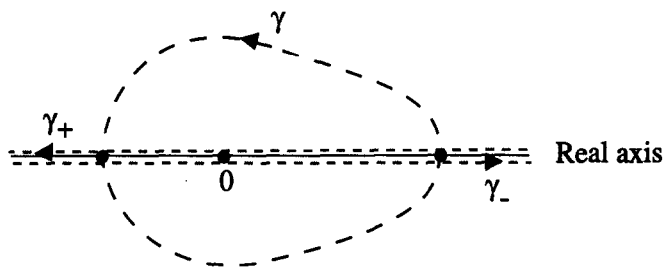


Figure 1. Shifting the path  $\gamma$  to  $\gamma_+ + \gamma_-$ .

Thus,

$$\delta(x) = -\frac{1}{2\pi i} \left( \frac{1}{x+i0} - \frac{1}{x-i0} \right)$$

is defined as the limit of two holomorphic functions, one holomorphic in the upper half-plane and the other holomorphic in the lower half-plane.

We write  $\mathbb{C}^2 = \mathbb{R}_x^2 + i\mathbb{R}_y^2$  and let  $\Gamma$  be a cone with vertex at the origin in  $\mathbb{R}_y^2$ . If  $\Delta$  is an open set in  $\mathbb{R}_y^2$  which approaches  $\Gamma$  asymptotically near the origin from the interior of  $\Gamma$ , then the subset  $U = \mathbb{R}^2 + i\Delta$  of  $\mathbb{C}^2$  is called an *infinitesimal wedge* with opening  $\Gamma$ , and is denoted by  $\mathbb{R}^2 + i\Gamma_0$  (see Figure 2).

Let  $f(x)$  be a "generalized boundary value" of a holomorphic function in an infinitesimal wedge  $\mathbb{R}^2 + i\Gamma_0$ ; that is,

$$f(x) = \lim_{\substack{y \rightarrow 0 \\ y \in \Gamma}} f(x + iy),$$

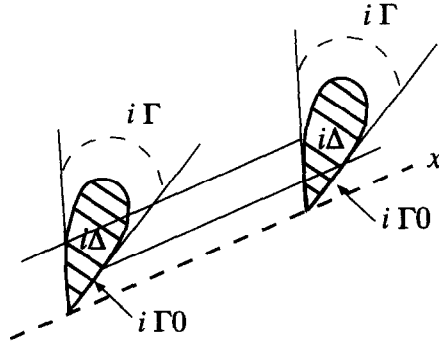


Figure 2. An infinitesimal wedge  $\mathbb{R}^2 + i\Gamma_0$ .

which, for simplicity, we write as

$$f(x) = f(x + i\Gamma_0).$$

Such a distribution can be thought of as being analytic with respect to the direction of  $\Gamma$ .

We are interested in the directional analyticity of a distribution [12,13].

**DEFINITION 1.** A distribution  $f(x)$  is said to be analytic with respect to a direction  $\xi_0$  if it can be represented as a finite sum of limits  $f_j(x + i\Gamma_j 0)$  of slowly increasing holomorphic functions  $f_j(z)$  in  $\mathbb{R}^2 + i\Gamma_j 0$  such that for every  $j$  we have

$$\Gamma_j \cap \{y \in \mathbb{R}^2; y \cdot \xi_0 < 0\} \neq \emptyset.$$

To characterize the microanalyticity of a slowly increasing distribution  $f \in S'(\mathbb{R}^2)$  by its Fourier transform  $\hat{f}$ , we introduce the dual cone,  $\Gamma^\circ$ , of  $\Gamma$  defined by

$$\Gamma^\circ := \{\xi \in \mathbb{R}^2; y \cdot \xi \geq 0, \text{ for every } y \in \Gamma\}$$

(see Figure 3). If  $\Gamma$  is a cone in  $\mathbb{R}^2$ , then the dual cone  $\Gamma^\circ$  is a closed convex cone in  $\mathbb{R}^2$ . Moreover,  $\Gamma^\circ$  is a proper cone. The complement of  $\Gamma^\circ$  is denoted by  $(\Gamma^\circ)^c$ .

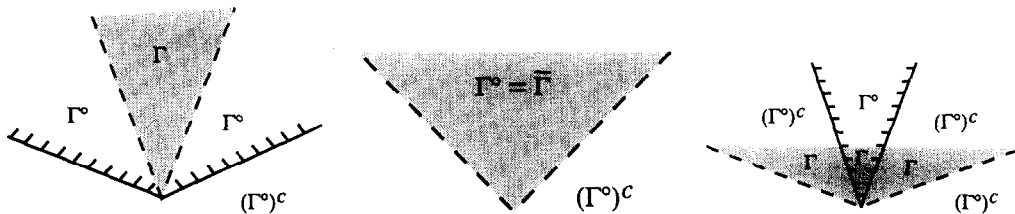


Figure 3. Open cone  $\Gamma$ , dual cone  $\Gamma^\circ$ , and complement  $(\Gamma^\circ)^c$  of dual cone.

The following two lemmas are standard (see [14]).

**LEMMA 1.** Let  $\Gamma$  be an open convex cone. A slowly increasing distribution  $f(x) \in S'(\mathbb{R}^2)$  can be represented as the limit  $f(x + i\Gamma_0)$  of a slowly increasing holomorphic function  $f(z)$  in the infinitesimal wedge  $\mathbb{R}^2 + i\Gamma_0$  if and only if the Fourier transform  $\hat{f}$  of  $f$  is exponentially decreasing in the open cone  $(\Gamma^\circ)^c$ , the complement of  $\Gamma^\circ$ ; that is,  $\hat{f}$  is exponentially decreasing on every closed proper subcone  $\Gamma' \subset\subset (\Gamma^\circ)^c$ .

The convex hull of an open cone  $\Gamma$  is denoted by  $\text{co}\Gamma$ . It can be shown that  $\Gamma^\circ = (\text{co}\Gamma)^\circ$ .

**LEMMA 2. (BOCHNER).** Let  $\Gamma$  be an open connected cone. Every slowly increasing holomorphic function in the infinitesimal wedge  $\mathbb{R}^2 + i\Gamma_0$  can be extended to a slowly increasing holomorphic function in the infinitesimal wedge  $\mathbb{R}^2 + i(\text{co}\Gamma)_0$ .

Hereafter, we shall always assume that the opening  $\Gamma$  of an infinitesimal wedge is convex. The larger the opening  $\Gamma$ , the more regular a slowly increasing distribution  $f(x + i\Gamma 0)$  will be. The largest opening  $\Gamma$  is the whole space, in which case  $f(x + i\Gamma 0)$  is analytic. The next largest possible openings  $\Gamma$  are half-spaces.

Let a slowly increasing distribution  $f(x)$  be analytic with respect to a direction  $\xi_0$ . Then, by Definition 1,  $f(x)$  can be represented as a finite sum of limits  $f_j(x + i\Gamma_j 0)$  of slowly increasing holomorphic functions in  $\mathbb{R}^2 + i\Gamma_j 0$  such that  $\Gamma_j \cap \{y \in \mathbb{R}^2; y \cdot \xi_0 < 0\} \neq \emptyset$  for each  $j$ . By Lemma 1, each Fourier transform  $\hat{f}_j(\xi)$  is exponentially decreasing in the open cone  $(\Gamma_j^c)^c$ . Since  $\xi_0 \notin \Gamma_j^c$ , there exists an open cone  $\Gamma$  containing  $\xi_0$  such that the Fourier transform  $\hat{f}(\xi) = \sum \hat{f}_j(\xi)$  is exponentially decreasing in  $\Gamma$ .

It is desirable to localize the directional decay of a function in  $\xi$ -space (Fourier domain), because local nonsmoothness of a function  $f$  in  $x$ -space corresponds to slow decay of the Fourier transform  $\hat{f}$  along some directions at infinity. Each such direction corresponds to a point on the unit sphere  $\mathbb{S}^1$  in  $\xi$ -space. Therefore, we shall use the coordinates  $(x, \xi) \in \mathbb{R}^2 \times \mathbb{S}^1$  to represent a point  $x \in \mathbb{R}^2$  together with a direction  $\xi \in \mathbb{S}^1$ .

**DEFINITION 2.** A distribution  $f(x) \in \mathcal{D}'(\mathbb{R}^2)$  is said to be analytic at  $x_0 \in \mathbb{R}^2$  if there exists an open neighborhood  $V \subset \mathbb{R}^2$  of  $x_0$  such that the restriction  $f|_V$  of  $f$  on  $V$  is analytic in  $V$ . The set of all points  $x \in \mathbb{R}^2$  where  $f$  is not analytic is called the singular support of  $f$ .

**DEFINITION 3.** A distribution  $f(x)$  is said to be microanalytic or microlocal analytic at  $(x_0, \xi_0) \in \mathbb{R}^2 \times \mathbb{S}^1$  if there exists a distribution  $g(x)$  which is analytic with respect to the direction  $\xi_0$  such that  $f(x) - g(x)$  is analytic in a neighborhood of  $x_0$ . The set of all points  $(x, \xi) \in \mathbb{R}^2 \times \mathbb{S}^1$  where  $f$  is not microanalytic is called the singular spectrum of  $f$ .

#### 4. NECESSARY AND SUFFICIENT CONDITIONS FOR TIGHT FRAME WAVELETS

We refer to [15,16] for detailed background on frames.

**DEFINITION 4.** Let  $I$  be an index set. A sequence of vectors  $\{f_i\}_{i \in I}$  in a Hilbert space  $H$  is called a frame for  $H$  if there exist constants  $A, B > 0$  (called frame bounds) such that

$$\forall f \in H, \quad A \|f\|^2 \leq \sum_{i \in I} |\langle f, f_i \rangle|^2 \leq B \|f\|^2.$$

If we can take  $A = B$ , then we say that the frame is an  $A$ -tight frame. If  $A = 1$ , then the 1-tight frame is called a Parseval frame.

It can be shown that  $\|f_i\|^2 \leq B$  for each  $i \in I$ . Further,  $\{f_i\}_{i \in I}$  is a tight frame with frame bound  $A$  if and only if

$$\forall f \in H, \quad \sum_{i \in I} \langle f, f_i \rangle f_i = Af.$$

All frames are complete (the finite linear span is dense in  $H$ ), but not all complete sets are frames. A frame is a basis for  $H$  if and only if it is a Riesz basis (the image of an orthonormal basis under a continuous, invertible mapping). A frame is *overcomplete* or *redundant* if it is possible to remove some element from the frame and still leave a complete set. For the case of tight frames, we can give the following easy characterization of redundancy. Redundancy of frames is explored in more detail in [17].

**LEMMA 3.** Let  $\{f_i\}_{i \in I}$  be an  $A$ -tight frame for a Hilbert space  $H$ . If  $j \in I$  is such that  $\|f_j\|^2 < A$ , then  $\{f_i\}_{i \neq j}$  is still a frame for  $H$ , with frame bounds  $A' = A - \|f_j\|^2$ ,  $B' = A$ .

**PROOF.** If  $f \in H$ , then clearly

$$\sum_{i \neq j} |\langle f, f_i \rangle|^2 \leq \sum_{i \in I} |\langle f, f_i \rangle|^2 = A \|f\|^2.$$

This establishes the upper frame bound. Also, using the Cauchy-Schwarz inequality, we have

$$\sum_{i \neq j} |\langle f, f_i \rangle|^2 = \sum_{i \in I} |\langle f, f_i \rangle|^2 - |\langle f, f_j \rangle|^2 \geq A \|f\|^2 - \|f\|^2 \|f_j\|^2 = (A - \|f_j\|^2) \|f\|^2,$$

which establishes the lower frame bound. ■

Given  $f \in L^2(\mathbb{R}^2)$ , let  $f_{j,k}(x)$  denote the scaled and shifted function

$$f_{j,k}(x) = 2^j f(2^j x - k), \quad j \in \mathbb{Z}, \quad k \in \mathbb{Z}^2. \tag{6}$$

Its Fourier transform is

$$\hat{f}_{j,k}(\xi) = e^{-2\pi i k \cdot \xi} 2^{-j} \hat{f}(2^{-j} \xi). \tag{7}$$

Let  $\mathbb{L}$  be a finite index set. A system  $\{\psi_{j,k}^\ell\}_{\ell \in \mathbb{L}, j \in \mathbb{Z}, k \in \mathbb{Z}^2} \subset L^2(\mathbb{R}^2)$  is called an *A-tight wavelet frame* if

$$f(x) = \frac{1}{A} \sum_{\substack{\ell \in \mathbb{L} \\ j \in \mathbb{Z} \\ k \in \mathbb{Z}^2}} \langle f, \psi_{j,k}^\ell \rangle \psi_{j,k}^\ell(x), \quad \forall f \in L^2(\mathbb{R}^2). \tag{8}$$

We recall that a system  $\{\psi_{j,k}^\ell\}_{\ell \in \mathbb{L}, j \in \mathbb{Z}, k \in \mathbb{Z}^2} \subset L^2(\mathbb{R}^2)$  is called an *orthonormal wavelet basis* if it is an orthonormal basis for  $L^2(\mathbb{R}^2)$ . An extension of Lemma 3 shows that this is equivalent to saying that the system  $\{\psi_{j,k}^\ell\}_{\ell \in \mathbb{L}, j \in \mathbb{Z}, k \in \mathbb{Z}^2}$  is a Parseval wavelet frame and  $\|\psi^\ell\|_{L^2(\mathbb{R}^2)} = 1$  for  $\ell \in \mathbb{L}$ .

The following general theorem, which is essentially Theorem 1 as stated and proved in [18] for  $\mathbb{R}^n$ , gives necessary and sufficient conditions to have a Parseval wavelet frame in  $\mathbb{R}^2$ .

**THEOREM 1.** *If  $\{\psi^1, \psi^2, \dots, \psi^L\} \subset L^2(\mathbb{R}^2)$ , then*

$$\|f\|_{L^2(\mathbb{R}^2)}^2 = \sum_{\substack{\ell \in \mathbb{L} \\ j \in \mathbb{Z} \\ k \in \mathbb{Z}^2}} |\langle f, \psi_{j,k}^\ell \rangle|^2, \tag{9}$$

for all  $f \in L^2(\mathbb{R}^2)$  if and only if the functions  $\{\psi^1, \psi^2, \dots, \psi^L\}$  satisfy the following two equalities:

$$\sum_{\substack{\ell \in \mathbb{L} \\ j \in \mathbb{Z}}} |\hat{\psi}^\ell(2^j \xi)|^2 = 1, \quad \text{a.e., } \xi \in \mathbb{R}^2, \tag{10}$$

$$\sum_{\substack{\ell \in \mathbb{L} \\ j \in \mathbb{Z}_+}} \hat{\psi}^\ell(2^j \xi) \overline{\hat{\psi}^\ell(2^j(\xi + q))} = 0, \quad \text{a.e., } \xi \in \mathbb{R}^2, \quad \forall q \in \mathbb{Z}^2 \setminus (2\mathbb{Z})^2, \tag{11}$$

where  $\mathbb{Z}_+ := \mathbb{N} \cup \{0\}$  and  $q \in \mathbb{Z}^2 \setminus (2\mathbb{Z})^2$  means that at least one component  $q_j$  is odd.

**COROLLARY 1.** *Under the hypotheses of Theorem 1, any function  $f \in L^2(\mathbb{R}^2)$  admits the tight wavelet frame expansion*

$$f(x) = \sum_{\substack{\ell \in \mathbb{L} \\ j \in \mathbb{Z} \\ k \in \mathbb{Z}^2}} \langle f, \psi_{j,k}^\ell \rangle \psi_{j,k}^\ell(x). \tag{12}$$

By using the localization property of the frame wavelet in the Fourier domain, one can study the directions of growth of  $\hat{f}(\xi)$  by looking at the size of the frame coefficients

$$\langle f, \psi_{j,k}^\ell \rangle = \langle \hat{f}, \hat{\psi}_{j,k}^\ell \rangle. \tag{13}$$

Moreover, by using the localization property of the frame wavelets in  $x$ -space, one can localize the singular support of  $f(x)$  by varying  $\ell$ ,  $j$ , and  $k$  in (13).

An alternate formulation of the problem is by means of a pseudodifferential operator

$$Pf(x) = \int e^{2\pi i \xi \cdot x} p(x, \xi) \hat{f}(\xi) d\xi. \tag{14}$$

The problem is to find a symbol  $p$  such that  $Pf$  is strongly localized on the singular support of  $f$  and negligible where  $f$  is smooth. Pseudodifferential operators with smooth symbols do not extend the singular support of  $f$ ; that is, the singular support of  $Pf$  is contained in the singular support of  $f$ . In Section 12, the symbol will involve only the matrix  $Q_j^2$  which will be a discretized version of  $\hat{\psi}_j^2(\xi) = \hat{\psi}^2(2^{-j}\xi)$ , and the values of the shift parameter  $k$  in the summation in (12) will be determined indirectly by the singular support of  $f$  through the size of  $|\langle \hat{f}, \hat{\psi}_{j,k}^2 \rangle|$ .

### 5. PAVING OF THE FOURIER DOMAIN FOR MICROLOCAL ANALYSIS

The localization property of the frame wavelets in the Fourier domain (13) will depend upon the support of the wavelet functions  $\hat{\psi}_{j,k}^\ell$  on appropriate rectangular or polar pavings of the plane.

Rectangular pavings of the Fourier domain in  $\mathbb{R}^2$  will consist of rings of 12 dyadic squares. Five “square” rings are shown in Figure 4 with artificially added spacing around the boxes for immediate visual perception.

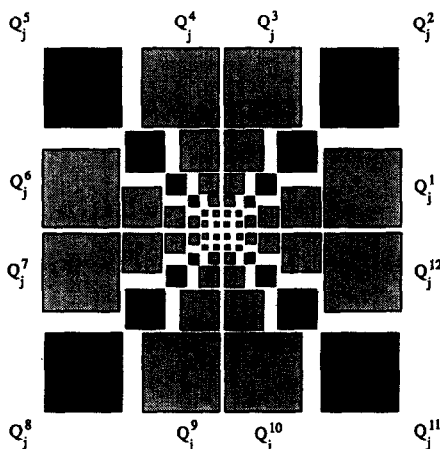


Figure 4. Five rings of 12 dyadic squares with four central black squares in the Fourier domain.

In the case of nonsmooth orthonormal box wavelets, the zeroth ring,  $\mathcal{R}^{[0]}$ , will consist of the 12 unit squares,  $Q_0^1, Q_0^2, \dots, Q_0^{12}$ , immediately surrounding the four black unit squares shown in Figure 4. The  $j^{\text{th}}$  ring  $\mathcal{R}^{[j]}$  consists of the squares  $Q_j^\ell$ ,  $\ell = 1, 2, \dots, 12$ , with sides of length  $2^j$ , obtained by dyadic scaling.

In the case of smooth frame wavelets, the central square will be a unit square made up of the four central black squares shown in Figure 4, and the zeroth ring,  $\mathcal{R}^{[0]}$ , will consist of the 12 squares with sides of length  $1/2$ , and the squares of the  $j^{\text{th}}$  ring will have sides of length  $2^{j-1}$ . Smaller squares will allow tapering of the scaling function and frame wavelets and still maintain the tightness of the frames.

To have arbitrarily fine angular resolutions in the Fourier domain, in Section 11, it will be convenient to consider polar pavings of the plane by dyadic sectors of annuli with unequal angular divisions, as shown in Figure 5.

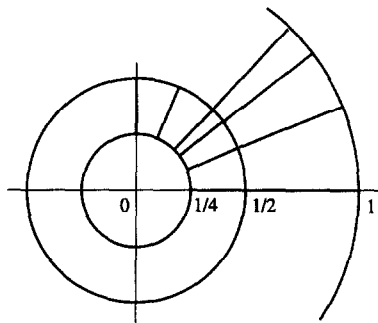


Figure 5. Dyadic sectors of annuli with central disk in the Fourier domain. Unequal angular divisions offer directional freedom.

## 6. MULTIREOLUTION ANALYSIS FOR WAVELETS WITH BOX FOURIER TRANSFORMS

This section is primarily concerned with a two-dimensional generalization of Examples I and K of [6, pp. 386,390].

Define the classical Hardy spaces  $H^2(\mathbb{R}_\pm)$  by

$$H^2(\mathbb{R}_\pm) = \left\{ f \in L^2(\mathbb{R}); \hat{f}(\xi) = 0 \text{ a.e., } \xi \leq (\geq) 0 \right\}.$$

In these examples, a scaling function  $\phi_+$  and a wavelet function  $\psi_+$  for orthonormal wavelets of  $H^2(\mathbb{R}_+)$  are defined by

$$\hat{\phi}_+ = \chi_{[0,1]}, \quad \hat{\psi}_+ = \chi_{[1,2]}.$$

From the two-scale relation

$$2\hat{\phi}_+(2\xi) = m_0(\xi)\hat{\phi}_+(\xi)$$

it is found that the corresponding lowpass filter is

$$m_0(\xi) = 2\chi_{[0,1/2]}(\xi) = 2\hat{\phi}_+(2\xi)$$

on  $[0, 1)$ , and extended 1-periodically to the line. From the two-scale relation

$$2\hat{\psi}_+(2\xi) = e^{2\pi i\xi} \overline{m_0\left(\xi + \frac{1}{2}\right)} \hat{\phi}_+(\xi) = m_1(\xi)\hat{\phi}_+(\xi)$$

it is found that the corresponding highpass filter is

$$m_1(\xi) = e^{2\pi i\xi} \overline{m_0\left(\xi + \frac{1}{2}\right)} = 2\hat{\psi}_+(2\xi)$$

on  $[0, 1)$ , and extended 1-periodically to the line.

By the same argument, we have a wavelet function  $\psi_-$  and a scaling function  $\phi_-$  for orthonormal wavelets of  $H^2(\mathbb{R}_-)$ . Since

$$L^2(\mathbb{R}) = H^2(\mathbb{R}_+) \oplus H^2(\mathbb{R}_-),$$

$\{\psi_+, \psi_-\}$  and  $\{\phi_+, \phi_-\}$  can be regarded as multiwavelet functions and multiscaling functions, respectively, of  $L^2(\mathbb{R})$ .

For the two-dimensional case, we can take the tensor product of multiresolution analyses for one-dimensional multiwavelets. Then the four multiscaling functions  $\phi^1, \phi^2, \phi^3, \phi^4$  are defined by their Fourier transforms,

$$\begin{aligned} \hat{\phi}^1(\xi_1, \xi_2) &:= \hat{\phi}_+(\xi_1)\hat{\phi}_+(\xi_2), & \hat{\phi}^2(\xi_1, \xi_2) &:= \hat{\phi}_-(\xi_1)\hat{\phi}_+(\xi_2), \\ \hat{\phi}^3(\xi_1, \xi_2) &:= \hat{\phi}_-(\xi_1)\hat{\phi}_-(\xi_2), & \hat{\phi}^4(\xi_1, \xi_2) &:= \hat{\phi}_+(\xi_1)\hat{\phi}_-(\xi_2), \end{aligned}$$

with support on the four central black unit squares, respectively, in Figure 4. To each multiscaling function, there correspond three multiwavelet functions. These 12 multiwavelet functions  $\psi^\ell$ ,  $\ell = 1, 2, \dots, 12$ , are

$$\begin{aligned}\hat{\psi}^1(\xi_1, \xi_2) &:= \hat{\psi}_+(\xi_1)\hat{\phi}_+(\xi_2), & \hat{\psi}^2(\xi_1, \xi_2) &:= \hat{\psi}_+(\xi_1)\hat{\psi}_+(\xi_2), \\ \hat{\psi}^3(\xi_1, \xi_2) &:= \hat{\phi}_+(\xi_1)\hat{\psi}_+(\xi_2), & \hat{\psi}^4(\xi_1, \xi_2) &:= \hat{\phi}_-(\xi_1)\hat{\psi}_+(\xi_2), \\ \hat{\psi}^5(\xi_1, \xi_2) &:= \hat{\psi}_-(\xi_1)\hat{\psi}_+(\xi_2), & \hat{\psi}^6(\xi_1, \xi_2) &:= \hat{\psi}_-(\xi_1)\hat{\phi}_+(\xi_2), \\ \hat{\psi}^7(\xi_1, \xi_2) &:= \hat{\psi}_-(\xi_1)\hat{\phi}_-(\xi_2), & \hat{\psi}^8(\xi_1, \xi_2) &:= \hat{\psi}_-(\xi_1)\hat{\psi}_-(\xi_2), \\ \hat{\psi}^9(\xi_1, \xi_2) &:= \hat{\phi}_-(\xi_1)\hat{\psi}_-(\xi_2), & \hat{\psi}^{10}(\xi_1, \xi_2) &:= \hat{\phi}_+(\xi_1)\hat{\psi}_-(\xi_2), \\ \hat{\psi}^{11}(\xi_1, \xi_2) &:= \hat{\psi}_+(\xi_1)\hat{\psi}_-(\xi_2), & \hat{\psi}^{12}(\xi_1, \xi_2) &:= \hat{\psi}_+(\xi_1)\hat{\phi}_-(\xi_2).\end{aligned}$$

The three families in quadrant  $\alpha$ ,  $\alpha = 1, 2, 3, 4$ , can be generated by the corresponding scaling function  $\phi^\alpha$ .

The scaling function satisfies the identity

$$\left| \hat{\phi}^\alpha(\xi) \right|^2 = \sum_{j=1}^{\infty} \sum_{\beta=1}^3 \left| \hat{\psi}^{3(\alpha-1)+\beta}(2^j\xi) \right|^2.$$

In this case, since the  $\hat{\psi}^\ell$  are characteristic functions of disjoint sets, we may remove the squares and the absolute values to get

$$\hat{\phi}^\alpha(\xi) = \sum_{j=1}^{\infty} \sum_{\beta=1}^3 \hat{\psi}^{3(\alpha-1)+\beta}(2^j\xi).$$

It follows that each  $\phi^\alpha$ ,  $\alpha = 1, 2, 3, 4$ , being the characteristic function of one of the four central squares in Figure 4, satisfies the two-scale equation

$$2\hat{\phi}^\alpha(2\xi) = m_0^\alpha(\xi)\hat{\phi}^\alpha(\xi) \quad (15)$$

with lowpass filter

$$m_0^\alpha(\xi) = 2\hat{\phi}^\alpha(2\xi) = \sum_{j=2}^{\infty} \sum_{\beta=1}^3 2\hat{\psi}^{3(\alpha-1)+\beta}(2^j\xi) = 2\chi_{\text{supp } \hat{\phi}^\alpha(2\cdot)}(\xi) \quad (16)$$

on  $[0, 1) \times [0, 1)$ , and extended  $(1 \times 1)$ -periodically to the plane. Then each wavelet  $\hat{\psi}^\ell$ ,  $\ell = 3(\alpha - 1) + \beta$ , where  $\alpha = 1, 2, 3, 4$ ,  $\beta = 1, 2, 3$ , satisfies the two-scale equation

$$2\hat{\psi}^\ell(2\xi) = m_1^\ell(\xi)\hat{\phi}^\alpha(\xi) \quad (17)$$

with highpass filter

$$m_1^\ell(\xi) = 2\hat{\psi}^\ell(2\xi) = 2\chi_{\text{supp } \hat{\psi}^\ell(2\cdot)}(\xi) \quad (18)$$

on  $[0, 1) \times [0, 1)$ , and extended  $(1 \times 1)$ -periodically to the plane. In this case, we have a genuine multiresolution analysis with box orthonormal scaling functions and wavelets.

Because of the form of the two-scale equations (15) and (17), and the lowpass and highpass filters (16) and (18), which are the periodized characteristic functions of the supports of  $\hat{\phi}^\alpha(2\xi)$  and  $\hat{\psi}^\ell(2\xi)$ , respectively, a multiwavelet multiresolution analysis could be generated by a single scaling function consisting of the characteristic function of the central unit square made of the four black squares in Figure 4.

Similarly, one can use 12 scaling functions of the form

$$\hat{\phi}^\ell(\xi) = \sum_{j=1}^{\infty} \hat{\psi}^\ell(2^j \xi),$$

with two-scale relation

$$2\hat{\phi}^\ell(2\xi) = m_0^\ell(\xi)\hat{\phi}^\ell(\xi)$$

and lowpass filter

$$m_0^\ell(\xi) = 2\hat{\phi}^\ell(2\xi) = \sum_{j=2}^{\infty} 2\hat{\psi}^\ell(2^j \xi) = 2\chi_{\text{supp } \hat{\phi}^\ell(2\cdot)}(\xi)$$

on  $[0, 1) \times [0, 1)$ , and extended  $(1 \times 1)$ -periodically to the plane. The wavelet  $\hat{\psi}^\ell$  satisfies the two-scale equation

$$2\hat{\psi}^\ell(2\xi) = m_1^\ell(\xi)\hat{\phi}^\ell(\xi)$$

with highpass filter

$$m_1^\ell(\xi) = 2\hat{\psi}^\ell(2\xi) = 2\chi_{\text{supp } \hat{\psi}^\ell(2\cdot)}(\xi)$$

on  $[0, 1) \times [0, 1)$ , and extended  $(1 \times 1)$ -periodically to the plane.

In the terminology of image processing, in all cases we have infinite impulse response filters.

### 7. PAINLESS SMOOTH TIGHT FRAME WAVELETS

The argument in this section is in the spirit of the one-dimensional tight frames given in [16], which are themselves derived from the construction in [19].

Let  $Q_0$  be the square  $[-1/2, 1/2] \times [-1/2, 1/2]$  centered at the origin and consider a “square” ring made of the 12 squares  $Q_1, \dots, Q_{12}$  with sides of length  $1/2$  surrounding the central unit square  $Q_0$  which is made of the four black squares shown in Figure 4.

Let  $\varepsilon$  be given such that  $0 < \varepsilon < 1/4$ , and let  $\tilde{Q}_\ell$  be an enlarged version of the square  $Q_\ell$  by at most a band of width  $\varepsilon$  along each side. For example, for  $Q_1 = [1/2, 1] \times [0, 1/2]$ ,

$$\tilde{Q}_1 = \left[ \frac{1}{2} - \varepsilon, 1 + \varepsilon \right] \times \left[ -\varepsilon, \frac{1}{2} + \varepsilon \right].$$

Let  $g_\ell \in L^2(\mathbb{R}^2)$  be such that:

- (1)  $\hat{g}_\ell$  is continuous,
- (2)  $\hat{g}_\ell$  is supported in  $\tilde{Q}_\ell$ ,
- (3)  $\hat{g}_\ell$  is nonzero in the interior of  $\tilde{Q}_\ell$ , and
- (4)  $\hat{g}_\ell$  is identically 1 on  $Q_\ell$ .

Define

$$G(\xi) = \sum_{\ell=1}^{12} \sum_{j=-\infty}^{\infty} |\hat{g}_\ell(2^{-j}\xi)|^2, \quad \xi \in \mathbb{R}^2. \tag{19}$$

For any given point  $\xi$ , there are only finitely many nonzero terms in the series in equation (19). Since each  $\hat{g}_\ell$  is bounded, then  $G$  is bounded above. For any given point  $\xi \neq 0$ , there is at least one term in equation (19) such that  $2^{-j}\xi$  lies in some  $Q_\ell$ . Hence,  $G(\xi) \geq 1$  except at the origin, where it is zero.

Define the functions

$$\hat{\psi}^\ell(\xi) = \frac{\hat{g}_\ell(\xi)}{\sqrt{G(\xi)}}, \quad \ell = 1, \dots, 12. \tag{20}$$

It is clear that  $\hat{\psi}^\ell(\xi)$  is in  $L^2(\mathbb{R}^2)$ . For each point  $\xi \neq 0$ , we have

$$\sum_{\ell=1}^{12} \sum_{j=-\infty}^{\infty} |\hat{\psi}^\ell(2^{-j}\xi)|^2 = 1 \tag{21}$$

since  $G$  is invariant under dyadic scaling. Note that this remains true even when  $G(\xi)$  is unbounded.

For  $k \in \mathbb{Z}^2$ , the functions

$$e_k(\xi) = e^{-2\pi i \xi \cdot k}, \quad \xi \in \mathbb{R}^2, \tag{22}$$

form an orthonormal basis for  $L^2((0, 1)^2)$ . The fact that  $\tilde{Q}_\ell$  is contained in a square with sides of length 1 will be used below.

As in (6), define the functions

$$\psi_{j,k}^\ell(x) = 2^j \psi^\ell(2^j x - k), \quad j \in \mathbb{Z}, \quad k \in \mathbb{Z}^2, \quad \ell = 1, \dots, 12. \tag{23}$$

Then

$$\hat{\psi}_{j,k}^\ell(\xi) = 2^{-j} e_k(2^{-j} \xi) \hat{\psi}^\ell(2^{-j} \xi). \tag{24}$$

Although it follows from Theorem 1 that  $\{\psi_{j,k}^\ell\}$  generates a Parseval frame, we give an independent proof, and also show that this frame is redundant.

**THEOREM 2.** *The functions  $\psi^1, \dots, \psi^{12}$  defined by (20) generate a redundant Parseval wavelet frame.*

**PROOF.** If  $Q$  is any unit square, then  $\{e_k; k \in \mathbb{Z}^2\}$  is an orthonormal basis for  $L^2(Q)$ . Hence, if  $S$  is a subset of a unit square  $Q$  then  $\{e_k; k \in \mathbb{Z}^2\}$  is a Parseval frame for  $L^2(S)$ . If  $S$  has measure less than 1, then this frame for  $L^2(S)$  is redundant. In particular, since  $\tilde{Q}_\ell$  is contained in a unit square, we therefore have by a change of variables that  $\{2^{-j} e_k(2^{-j} \xi); k \in \mathbb{Z}^2\}$  is a Parseval frame for  $L^2(2^j \tilde{Q}_\ell)$ . Using this tight frame and also Plancherel's theorem, we can therefore calculate that, for any  $f \in L^2(\mathbb{R}^2)$ , we have

$$\begin{aligned} \sum_{k \in \mathbb{Z}^2} |\langle f, \psi_{j,k}^\ell \rangle|^2 &= \sum_{k \in \mathbb{Z}^2} |\langle \hat{f}, \hat{\psi}_{j,k}^\ell \rangle|^2 \\ &= \sum_{k \in \mathbb{Z}^2} \left| \int \hat{f}(\xi) \overline{\hat{\psi}^\ell(2^{-j} \xi)} 2^{-j} e_{-k}(2^{-j} \xi) d\xi \right|^2 \\ &= \sum_{k \in \mathbb{Z}^2} \left| \langle \hat{f}(\xi) \overline{\hat{\psi}^\ell(2^{-j} \xi)}, 2^{-j} e_{-k}(2^{-j} \xi) \rangle_{L^2(2^j \tilde{Q}_\ell)} \right|^2 \\ &= \int |\hat{f}(\xi)|^2 |\hat{\psi}^\ell(2^{-j} \xi)|^2 d\xi. \end{aligned}$$

Consequently,

$$\begin{aligned} \sum_{\ell=1}^{12} \sum_{j=-\infty}^{\infty} \sum_{k \in \mathbb{Z}^2} |\langle f, \psi_{j,k}^\ell \rangle|^2 &= \sum_{\ell=1}^{12} \sum_{j=-\infty}^{\infty} \int |\hat{f}(\xi)|^2 |\hat{\psi}^\ell(2^{-j} \xi)|^2 d\xi \\ &= \int |\hat{f}(\xi)|^2 \left( \sum_{\ell=1}^{12} \sum_{j=-\infty}^{\infty} |\hat{\psi}^\ell(2^{-j} \xi)|^2 \right) d\xi \\ &= \int |\hat{f}(\xi)|^2 d\xi \\ &= \|f\|_{L^2(\mathbb{R}^2)}^2. \end{aligned}$$

Thus,  $\{\psi_{j,k}^\ell\}_{j \in \mathbb{Z}, k \in \mathbb{Z}^2, \ell=1, \dots, 12}$  is a Parseval wavelet frame for  $L^2(\mathbb{R}^2)$ .

To show that this frame is redundant, it suffices, by Lemma 3, to show that  $\|\psi^\ell\|_{L^2(\mathbb{R}^2)} < 1$  for some  $\ell$ . In fact, this is true for every  $\ell$ . For simplicity, consider  $\ell = 1$ . We have  $\hat{\psi}^1$  supported within  $\tilde{Q}_1 = [1/2 - \varepsilon, 1 + \varepsilon] \times [-\varepsilon, 1/2 + \varepsilon]$ , which is itself contained within the unit square  $Q =$

$[1/4, 5/4] \times [-1/4, 3/4]$ . Further, by construction we have that  $\hat{\psi}^1$  is continuous,  $0 \leq |\hat{\psi}^1(\omega)| \leq 1$  for all  $\omega$ , and  $\hat{\psi}^1(\omega) = 0$  for  $\omega \in \partial Q$ . It follows directly then that  $\|\psi^1\|_{L^2(\mathbb{R}^2)}^2 = \int |\hat{\psi}^1(\omega)|^2 d\omega < 1$ , which completes the proof. ■

Let  $\mathbb{L} = \{1, \dots, 12\}$ . In fact, once we know that the frame  $\{\psi_{j,k}^\ell\}_{(j,k,\ell) \in \mathbb{Z} \times \mathbb{Z}^2 \times \mathbb{L}}$  is redundant, it follows from [17, Theorem 6.8] that there exists a set  $J$  of infinite cardinality such that  $\{\psi_{j,k}^\ell\}_{(j,k,\ell) \in (\mathbb{Z} \times \mathbb{Z}^2 \times \mathbb{L}) \setminus J}$  is still a frame for  $L^2(\mathbb{R}^2)$ .

### 8. RINGS OF 12 TAPERED FRAME WAVELETS

In this section, we construct smooth tight frame wavelets satisfying (1) identically. This fact accelerates computation in the construction of frames in view of the numerical implementations in Section 12.

We first define bell functions of one variable. We partition the  $s$ -axis with points  $\{a_j\}$  ( $a_j < a_{j+1}$ ) into intervals, such that the  $j^{\text{th}}$  interval is  $[a_j, a_{j+1}]$  and has length  $L_j = a_{j+1} - a_j$ . Around each endpoint of an interval, say  $a_j$ , we allow a *transition region*  $[a_j - \varepsilon_j, a_j + \varepsilon_j]$  of width  $2\varepsilon_j$ ; in this region, the bell function  $b_j(s)$  over the interval  $j$  rises smoothly from 0 to 1, and the bell function  $b_{j-1}(s)$  over the interval  $j - 1$  decreases smoothly from 1 to 0. The bell function  $b_j(s)$  is nonzero for  $s$  in the region  $(a_j - \varepsilon_j, a_{j+1} + \varepsilon_{j+1})$  and it is 1 for  $s$  in  $[a_j + \varepsilon_j, a_{j+1} - \varepsilon_{j+1}]$ . Bell functions over two adjacent intervals overlap in the transition region.

A bell function, or window,  $b_j(s)$  has the following properties:

- (i)  $0 \leq b_j(s) \leq 1$  for all  $s$  and

$$b_j(s) = \begin{cases} 1, & \text{if } a_j + \varepsilon_j \leq s \leq a_{j+1} - \varepsilon_{j+1}, \\ 0, & \text{if } s \leq a_j - \varepsilon_j \text{ or } s \geq a_{j+1} + \varepsilon_{j+1}, \end{cases}$$

where  $\varepsilon_j \geq 0$  and  $\varepsilon_j + \varepsilon_{j+1} \leq L_j$ ;

- (ii)  $b_j^2(a_j + s) + b_j^2(a_j - s) = 1$  if  $|s| \leq \varepsilon_j$ ;
- (iii)  $b_j(a_j + s) = b_{j-1}(a_j - s)$  if  $|s| \leq \varepsilon_j$ .

We notice that Condition (i) says that the windows are simply smoothed versions of the rectangular window and  $b_j$  can be specified if it is known in the left transition region  $\text{LTR} = [a_j - \varepsilon_j, a_j + \varepsilon_j]$  and the right transition region  $\text{RTR} = [a_{j+1} - \varepsilon_{j+1}, a_{j+1} + \varepsilon_{j+1}]$ . So we need only consider the window function in the transition regions; we refer to this as a *taper function*. We shall denote the restrictions of  $b_j$  on LTR and RTR by

$$t_l(s; \varepsilon_j) = b_j(s), \quad \text{for } s \in [a_j - \varepsilon_j, a_j + \varepsilon_j], \tag{25}$$

and

$$t_r(s; \varepsilon_j) = b_j(s), \quad \text{for } s \in [a_{j+1} - \varepsilon_{j+1}, a_{j+1} + \varepsilon_{j+1}], \tag{26}$$

respectively.

The left part of Figure 6 shows three tapered characteristic functions:

- (a) of the interval  $[0, 1]$  with transition width  $1/2$  at both ends,
- (b) of the interval  $[1, 2]$  with transition widths  $1/2$  at the left end and  $1$  at the right end, and
- (c) of the interval  $[2, 4]$  with transition widths  $1$  at the left end and  $2$  at the right end.

It is seen in the right part of Figure 6 that the square root of the sum of the squares of these three functions is equal to 1 over the overlapping tapered parts.

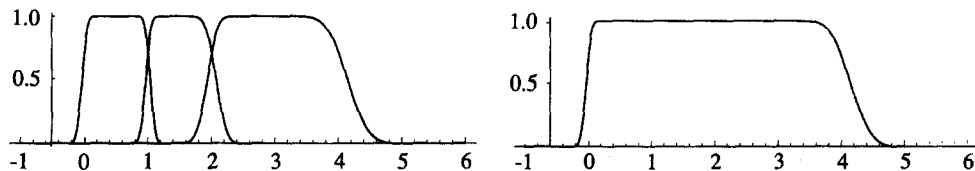


Figure 6. Left: three overlapping tapered characteristic functions. Right: square root of sum of squares of the three functions.

Bell functions of two variables are defined as the tensor product of two bell functions of one variable,

$$b(s_1, s_2) = b_1(s_1)b_2(s_2),$$

where  $b_1$  and  $b_2$  have transition regions of appropriate lengths at their left and right ends. The tapered characteristic functions of the 12 squares of side  $1/2$  of the ring  $\mathcal{R}^{[0]}$ , shown in Figure 7, have transition widths  $4\epsilon$  on the outside edges and  $2\epsilon$  on all the other edges. Similarly, the three squares of side 1 of the second ring  $\mathcal{R}^{[1]}$  in the first quadrant, produced by dilation by 2, have transition widths  $8\epsilon$  on the four outside edges and  $4\epsilon$  on the remaining edges.

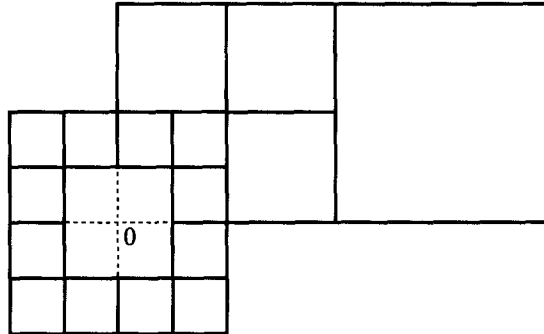


Figure 7. Twelve squares with sides of length  $1/2$  forming ring  $\mathcal{R}^{[0]}$ , and, in the first quadrant, three squares with sides of length 1 of ring  $\mathcal{R}^{[1]}$ , and one square with sides of length 2 of ring  $\mathcal{R}^{[2]}$ .

In general, the ring  $\mathcal{R}^{[j]}$ , parameterized by  $j \in \mathbb{Z}$ , is the support of tapered characteristic functions

$$\hat{\psi}_j^\ell(\xi) := \hat{\psi}^\ell(2^j\xi), \quad \ell = 1, 2, \dots, 12,$$

where the Fourier transform is defined by (2). For fixed  $j$ , the only rings that intersect with  $\mathcal{R}^{[j]}$  are  $\mathcal{R}^{[j-1]}$  and  $\mathcal{R}^{[j+1]}$ . Given one ring  $\mathcal{R}^{[j]}$ , the other rings are simply obtained by dilation.

To prove identity (1), one needs only check points where two, three, and four tapered wavelet frame functions overlap. Let us check identity (1) at an arbitrary point  $\xi$  in the intersection of the four tapered parts of  $\hat{\psi}_1^2$  and  $\hat{\psi}_2^2$ ,  $\ell = 1, 2, 3$ . Since tapering is of the same width for all four transition regions, it is obtained by the same taper functions (25) and (26),  $t_l(s, \epsilon)$  and  $t_r(s, \epsilon)$ , respectively. Proceeding counterclockwise from the top right corner of the frame  $\hat{\psi}_1^2$ , we have

$$\begin{aligned} & t_r(\xi, \epsilon)^2 t_r(\xi, \epsilon)^2 + t_r(\xi, \epsilon)^2 t_l(\xi, \epsilon)^2 + t_l(\xi, \epsilon)^2 t_l(\xi, \epsilon)^2 + t_l(\xi, \epsilon)^2 t_r(\xi, \epsilon)^2 \\ &= t_r(\xi, \epsilon)^2 [t_r(\xi, \epsilon)^2 + t_l(\xi, \epsilon)^2] + t_l(\xi, \epsilon)^2 [t_l(\xi, \epsilon)^2 + t_r(\xi, \epsilon)^2] \\ &= t_r(\xi, \epsilon)^2 + t_l(\xi, \epsilon)^2 \\ &= 1. \end{aligned}$$

We generalize to two dimensions the treatment of smooth frames for  $H^2(\mathbb{R})$  given in Section 8.4 of [6] and show that the  $\psi_{j,k}^\ell$  form a Parseval wavelet frame for  $L^2(\mathbb{R}^2)$ .

**THEOREM 3.** *If  $0 < \epsilon \leq 1/4$ , the system  $\{\psi_{j,k}^\ell\}$ ,  $j \in \mathbb{Z}$ , and  $k \in \mathbb{Z}^2$ , is a Parseval wavelet frame for  $L^2(\mathbb{R}^2)$ .*

**PROOF.** Identity (1) has just been proved. For  $f \in L^2(\mathbb{R}^2)$ , a similar argument to the proof of Theorem 2 implies

$$\sum_{k \in \mathbb{Z}^2} |\langle f, \psi_{j,k}^\ell \rangle|^2 = \int |\hat{f}(\xi)|^2 |\hat{\psi}^\ell(2^{-j}\xi)|^2 d\xi$$

and

$$\sum_{\ell=1}^{12} \sum_{j=-\infty}^{\infty} \sum_{k \in \mathbb{Z}^2} |\langle f, \psi_{j,k}^\ell \rangle|^2 = \sum_{\ell=1}^{12} \sum_{j=-\infty}^{\infty} \int |\hat{f}(\xi)|^2 |\hat{\psi}^\ell(2^{-j}\xi)|^2 d\xi = \int |\hat{f}(\xi)|^2 d\xi = \|f\|_{L^2(\mathbb{R}^2)}^2.$$

A “folding argument” [6, p. 419] shows that

$$\|\psi_{0,0}^\ell\|_{L^2(\mathbb{R}^2)}^2 = \frac{1}{4}.$$

Thus, we have a family of frames in  $L^2(\mathbb{R}^2)$  that do not form an orthonormal basis.

A finer angular localization in the Fourier domain is achieved by rings of 48 wavelet frame functions by dividing each of the previous 12 squares into four squares as shown in the left part of Figure 8. These functions are tapered and have transition widths  $4\varepsilon$  on the outside edges and  $2\varepsilon$  on all the other edges. It is easy to see that identity (1) is satisfied.

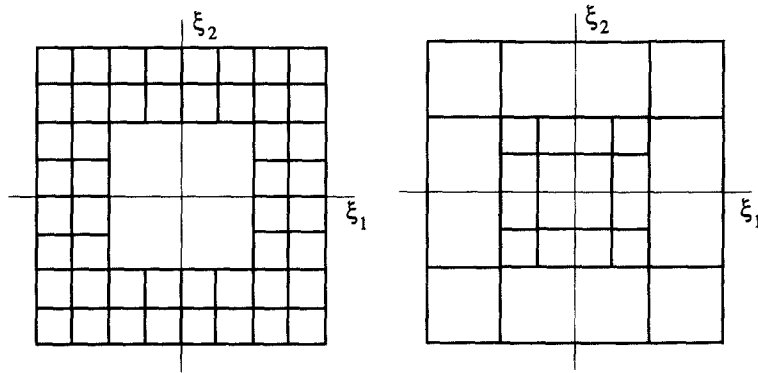


Figure 8. Left: One ring of 48 wavelet frame functions in the Fourier domain. Right: Two rings of eight wavelet frame functions in the Fourier domain.

Similarly, a coarser angular localization is achieved by rings of eight wavelet frame functions supported on rings of eight rectangles. Two such rings are shown in the right part of Figure 8 (see [20, p. 309]).

### 9. MULTIREOLUTION ANALYSIS FOR SMOOTH RECTANGULAR FRAME WAVELETS

We construct an orthonormal scaling function for our tapered rectangular frame wavelets. The smooth wavelets are obtained from the scaling function by a two-scale equation. However, the  $(1 \times 1)$ -periodic highpass filter will not be continuous over the basic unit square.

We recall that a *multiresolution analysis* consists of a sequence of closed subspaces  $\{V_j\}_{j \in \mathbb{Z}}$  of  $L^2(\mathbb{R}^2)$  satisfying the five requirements:

- (i)  $V_j \subset V_{j+1}$ , for all  $j \in \mathbb{Z}$ ;
- (ii)  $f(\cdot) \in V_j$  if and only if  $f(2\cdot) \in V_{j+1}$ , for all  $j \in \mathbb{Z}$ ;
- (iii)  $\bigcap_{j \in \mathbb{Z}} V_j = \{0\}$ ;
- (iv)  $\bigcup_{j \in \mathbb{Z}} V_j = L^2(\mathbb{R}^2)$ ;
- (v) there exists a function  $\phi \in V_0$  such that  $\{\phi(\cdot - k)\}_{k \in \mathbb{Z}^2}$  is an orthonormal basis for  $V_0$ .

Let  $b_\varepsilon$  be a tapered characteristic function of the unit interval  $[-1/2, 1/2]$  with transition regions of length  $2\varepsilon$ . We take for the scaling function the tapered characteristic function of the unit square with center at the origin,

$$\hat{\phi}(\xi_1, \xi_2) = b_\varepsilon(\xi_1)b_\varepsilon(\xi_2) \tag{27}$$

and transition regions of width  $2\varepsilon$ . Then we have the following Theorem 4.

**THEOREM 4.** *The tapered rectangular frame wavelet system defined in Section 8 is obtained from a multiresolution analysis of  $L^2(\mathbb{R}^2)$ .*

To prove Theorem 4, we shall use the following two lemmas.

**LEMMA 4.** *The smooth scaling function defined by (27) is an orthonormal scaling function.*

**PROOF.** We show first that the function  $\phi$ , defined by (27), is a scaling function for a multiresolution analysis if it satisfies the three conditions

- (a)  $\sum_{k \in \mathbb{Z}^2} |\hat{\phi}(\xi + k)|^2 = 1$ , a.e.,  $\xi \in [0, 1]^2$ ,
- (b)  $\lim_{j \rightarrow \infty} |\hat{\phi}(2^{-j}\xi)| = 1$ , a.e.,  $\xi \in \mathbb{R}^2$ , and
- (c) there exists a  $(1 \times 1)$ -periodic function  $m_0$  such that

$$2\hat{\phi}(2\xi) = m_0(\xi)\hat{\phi}(\xi), \quad \text{a.e., } \xi \in \mathbb{R}^2. \tag{28}$$

Condition (a) is equivalent to the fact that the system  $\{\phi(\cdot - k)\}_{k \in \mathbb{Z}^2}$  is orthonormal. If we define

$$V_0 := \overline{\text{Span}\{\phi(\cdot - k)\}_{k \in \mathbb{Z}^2}},$$

then requirement (v) is satisfied. If we define

$$V_j := \overline{\text{Span}\{2^j\phi(2^j \cdot - k)\}_{k \in \mathbb{Z}^2}},$$

then requirement (ii) is satisfied. Condition (c) implies requirement (i). Since  $\hat{\phi}$  has compact support, we can assume that  $\text{supp } \hat{\phi} \subset \{\xi; |\xi| < R\}$  for a positive  $R$ . For a function  $f \in V_j$ , there exists a function  $m_f(\xi) \in L^2([0, 1]^2)$  such that

$$\hat{f}(\xi) = m_f(2^{-j}\xi)\hat{\phi}(2^{-j}\xi).$$

This equality implies that

$$\text{supp } \hat{f}(\xi) \subset \text{supp } \hat{\phi}(2^{-j}\xi) \subset \{\xi; |\xi| < 2^j R\}.$$

Hence,  $f \in \bigcap_{j \in \mathbb{Z}} V_j$  implies that

$$\text{supp } \hat{f}(\xi) \subset \bigcap_{j \in \mathbb{Z}} \{\xi; |\xi| < 2^j R\} = \{0\}.$$

Thus, we have  $f = 0$ , a.e.  $\xi \in \mathbb{R}^2$ , which is requirement (iii).

To establish requirement (iv), it suffices to show that  $f \in \mathcal{F}^{-1}[C_0^\infty(\mathbb{R}^2)]$  is approximated by an element of  $\bigcup_{j \in \mathbb{Z}} V_j$ . Denote by  $P_j$  the orthogonal projection from  $L^2(\mathbb{R}^2)$  to  $V_j$ . Then it suffices to show that

$$\|P_j f - f\|^2 = \|f\|^2 - \|P_j f\|^2 \rightarrow 0, \quad f \in \mathcal{F}^{-1}[C_0^\infty(\mathbb{R}^2)],$$

as  $j \rightarrow \infty$ . For  $f \in \mathcal{F}^{-1}[C_0^\infty(\mathbb{R}^2)]$ , there exists  $J \in \mathbb{N}$  such that  $\text{supp } \hat{f}(2^j\xi) \subset [-1/2, 1/2]^2$ . Thus,

$$\begin{aligned} \|P_j f\|^2 &= \sum_{k \in \mathbb{Z}^2} |\langle f, 2^j\phi(2^j \cdot - k) \rangle|^2 \\ &= \sum_{k \in \mathbb{Z}^2} \left| \int_{\mathbb{R}^2} f(x) \overline{2^j\phi(2^j x - k)} dx \right|^2 \\ &= \sum_{k \in \mathbb{Z}^2} \left| 2^{-j} \int_{\mathbb{R}^2} f(2^{-j}y) \overline{\phi(y - k)} dy \right|^2 \\ &= \sum_{k \in \mathbb{Z}^2} \left| 2^j \int_{[-1/2, 1/2]^2} e^{2\pi i k \xi} \hat{f}(2^j\xi) \overline{\hat{\phi}(\xi)} d\xi \right|^2 \\ &= 2^{2j} \left\| \hat{f}(2^j \cdot) \overline{\hat{\phi}(\cdot)} \right\|_{L^2([-1/2, 1/2]^2)}^2 \\ &= \left\| \hat{f}(\cdot) \overline{\hat{\phi}(2^{-j} \cdot)} \right\|_{L^2(\mathbb{R}^2)}^2. \end{aligned}$$

Since  $|\hat{\phi}(\xi)| \leq 1$  by (a), Lebesgue's dominated convergence theorem can be applied. Thus, (b) implies that

$$\lim_{j \rightarrow \infty} \left\| \hat{f}(\cdot) \overline{\hat{\phi}(2^{-j}\cdot)} \right\|_{L^2(\mathbb{R}^2)}^2 = \left\| \hat{f} \right\|_{L^2(\mathbb{R}^2)}^2 = \|f\|_{L^2(\mathbb{R}^2)}^2.$$

The function  $\hat{\phi}(\xi)$  satisfies identity (a) because of the consistent tapering of the characteristic function of the unit square  $Q = [-1/2, 1/2] \times [-1/2, 1/2]$ .

Since  $\hat{\phi}$  is continuous and  $\hat{\phi}(\xi) \equiv 1$  in a neighborhood of the origin, we have

$$\lim_{j \rightarrow \infty} \hat{\phi}(2^{-j}\xi) = \hat{\phi}\left(\lim_{j \rightarrow \infty} 2^{-j}\xi\right) = 1,$$

for every  $\xi \in \mathbb{R}^2$ , and this implies (b).

Since the function  $\hat{\phi}(2\cdot)$  is supported on the square

$$\tilde{Q} = \left[-\frac{1}{4} - \frac{\varepsilon}{2}, \frac{1}{4} + \frac{\varepsilon}{2}\right) \times \left[-\frac{1}{4} - \frac{\varepsilon}{2}, \frac{1}{4} + \frac{\varepsilon}{2}\right),$$

the lowpass filter  $m_0$ , defined by

$$m_0(\xi) = \begin{cases} 2\hat{\phi}(2\xi), & \text{on } \tilde{Q}, \\ 0, & \text{on } Q \setminus \tilde{Q}, \end{cases}$$

and extended  $(1 \times 1)$ -periodically, is a smooth periodic function. It follows that the Fourier transform of the scaling function  $\phi$  satisfies the two-scale equation (28). ■

LEMMA 5. *There exist discontinuous  $(1 \times 1)$ -periodic functions  $m_\ell^1$ ,  $\ell = 1, 2, \dots, 12$ , such that the tapered rectangular frame wavelets defined in Section 8 satisfy the two-scale equations*

$$2\hat{\psi}^\ell(2\xi) = m_\ell^1(\xi)\hat{\phi}(\xi), \quad \text{a.e., } \xi \in \mathbb{R}^2, \quad \ell = 1, 2, \dots, 12. \tag{29}$$

PROOF. By symmetry, we need only consider two wavelets, namely  $\hat{\psi}^1(\xi)$  and  $\hat{\psi}^2(\xi)$ , since the other wavelets are obtained by left-right and up-down reflections. The wavelet  $\hat{\psi}^1(\xi)$  satisfies the two-scale equation

$$2\hat{\psi}^1(2\xi) = m_1^1(\xi)\hat{\phi}(\xi),$$

where the highpass filter,  $m_1^1(\xi)$ , is defined as follows.

On the rectangle

$$R_1^1 = \left\{ \frac{1}{4} - \frac{\varepsilon}{2} \leq \xi_1 \leq \frac{1}{2} - \varepsilon, -\frac{\varepsilon}{2} \leq \xi_2 \leq \frac{1}{4} + \frac{\varepsilon}{2} \right\},$$

where  $\hat{\phi}$  is equal to 1, define

$$m_1^1(\xi) = 2\hat{\psi}^1(2\xi), \quad \xi \in R_1^1.$$

On the rectangular transition region

$$R_2^1 = \left\{ \frac{1}{2} - \varepsilon \leq \xi_1 \leq \frac{1}{2} + \varepsilon, \frac{\varepsilon}{2} \leq \xi_2 \leq \frac{1}{4} - \frac{\varepsilon}{2} \right\},$$

where the taperings of  $\hat{\phi}(\xi)$  and  $\hat{\psi}^1(2\xi)$  coincide, define

$$m_1^1(\xi) = 2, \quad \xi \in R_2^1.$$

On the lower-right little rectangle

$$R_3^1 = \left\{ \frac{1}{2} - \varepsilon \leq \xi_1 \leq \frac{1}{2} + \varepsilon, -\frac{\varepsilon}{2} \leq \xi_2 \leq \frac{\varepsilon}{2} \right\},$$

where

$$\hat{\phi}(\xi_1, \xi_2) = t_r(\xi_1; \varepsilon)$$

and

$$\hat{\psi}(2\xi_1, 2\xi_2) = t_r(\xi_1; \varepsilon)t_l\left(\xi_2; \frac{\varepsilon}{2}\right),$$

define

$$m_1^1(\xi_1, \xi_2) = 2t_l\left(\xi_2; \frac{\varepsilon}{2}\right), \quad \xi \in R_3^1.$$

Similarly, on the upper-right little rectangle

$$R_4^1 = \left\{ \frac{1}{2} - \varepsilon \leq \xi_1 \leq \frac{1}{2} + \varepsilon, \frac{1}{4} - \frac{\varepsilon}{2} \leq \xi_2 \leq \frac{1}{4} + \frac{\varepsilon}{2} \right\},$$

where

$$\hat{\phi}(\xi_1, \xi_2) = t_r(\xi_1; \varepsilon)$$

and

$$\hat{\psi}^1(2\xi_1, 2\xi_2) = t_r(\xi_1; \varepsilon)t_r\left(\xi_2; \frac{\varepsilon}{2}\right),$$

define

$$m_1^1(\xi_1, \xi_2) = 2t_r\left(\xi_2; \frac{\varepsilon}{2}\right), \quad \xi \in R_4^1.$$

The wavelet  $\hat{\psi}^2(\xi)$  satisfies the two-scale equation

$$2\hat{\psi}^2(2\xi) = m_1^2(\xi)\hat{\phi}(\xi),$$

where the highpass filter,  $m_1^2(\xi)$ , is defined as follows.

On the square

$$R_1^2 = \left\{ \frac{1}{4} - \frac{\varepsilon}{2} \leq \xi_1 \leq \frac{1}{2} - \varepsilon, \frac{1}{4} - \frac{\varepsilon}{2} \leq \xi_2 \leq \frac{1}{2} - \varepsilon \right\},$$

where  $\hat{\phi}$  is equal to 1, define

$$m_1^2(\xi) = 2\hat{\psi}(2\xi), \quad \xi \in R_1^2.$$

On the union of the two rectangular transition regions

$$R_2^2 = \left\{ \frac{1}{2} - \varepsilon \leq \xi_1 \leq \frac{1}{2} + \varepsilon, \frac{1}{4} + \frac{\varepsilon}{2} \leq \xi_2 \leq \frac{1}{2} - \varepsilon \right\} \\ \cup \left\{ \frac{1}{4} - \frac{\varepsilon}{2} \leq \xi_1 \leq \frac{1}{2} - \varepsilon, \frac{1}{2} - \varepsilon \leq \xi_2 \leq \frac{1}{2} + \varepsilon \right\},$$

where the taperings of  $\hat{\phi}(\xi)$  and  $\hat{\psi}^2(2\xi)$  coincide, define

$$m_1^2(\xi) = 2, \quad \xi \in R_2^2.$$

On the lower-right little rectangle

$$R_3^2 = \left\{ \frac{1}{2} - \varepsilon \leq \xi_1 \leq \frac{1}{2} + \varepsilon, \frac{1}{4} - \frac{\varepsilon}{2} \leq \xi_2 \leq \frac{1}{4} + \frac{\varepsilon}{2} \right\},$$

where

$$\hat{\phi}(\xi_1, \xi_2) = t_r(\xi_1; \varepsilon)$$

and

$$\hat{\psi}(2\xi_1, 2\xi_2) = t_r(\xi_1; \varepsilon)t_l\left(\xi_2; \frac{\varepsilon}{2}\right),$$

define

$$m_1^2(\xi_1, \xi_2) = 2t_l \left( \xi_2, \frac{\varepsilon}{2} \right), \quad \xi \in R_3^2.$$

Similarly, on the upper-right little square,

$$R_4^2 = \left\{ \frac{1}{2} - \varepsilon \leq \xi_1 \leq \frac{1}{2} + \varepsilon, \frac{1}{2} - \varepsilon \leq \xi_2 \leq \frac{1}{2} + \varepsilon \right\},$$

where

$$\hat{\psi}^2(2\xi_1, 2\xi_2) = \hat{\phi}(\xi_1, \xi_2) = t_r(\xi_1; \varepsilon)t_r(\xi_2; \varepsilon),$$

define

$$m_1^2(\xi_1, \xi_2) = 2.$$

Hence, one sees that in all cases

$$m_1^\ell(\xi) = \frac{2\hat{\psi}^\ell(2\xi)}{\hat{\phi}(\xi)}, \quad \ell = 1, 2, \dots, 12,$$

over the support of  $\hat{\psi}^\ell(2\cdot)$  and zero elsewhere in the unit square. ■

PROOF OF THEOREM 4. The frames in Section 8 are Parseval wavelet frames. Lemmas 4 and 5 show that the  $\{\psi^\ell\}_{\ell \in \mathbb{L}}$  are obtained from a multiresolution analysis. ■

### 10. GENERAL CONSTRUCTION OF MICROLOCAL FRAME WAVELETS

The construction of smooth rectangular frame wavelets in the Fourier domain can be generalized to functions  $\hat{f}$  supported on a general ring of sets surrounding the origin and whose dyadic dilations cover  $\mathbb{R}^2 \setminus \{0\}$ . There is a ring, each function of which has support in a square with sides of length 1, so that a shift by 1 in any direction will result in nonoverlap with the unshifted function, and hence, equality (11) is satisfied. Thus, we obtain a tight wavelet frame by Theorem 1. Moreover, if equality (10) holds, the frame bound is equal to 1. But, in this case, the same result can be simply obtained by considering an orthonormal basis

$$e^{2\pi i k \cdot \xi}, \quad k \in \mathbb{Z}^2,$$

of a square with sides of length 1 and applying Plancherel's theorem. This simpler argument was used in Section 9 on painless smooth tight frame wavelets.

Given functions  $\hat{\psi}^\ell(\xi)$  as described above, define the real, nonnegative function  $\hat{\phi}(\xi)$  by the identity

$$|\hat{\phi}(\xi)|^2 = \sum_{j=1}^{\infty} \sum_{\ell=1}^L |\hat{\psi}^\ell(2^j \xi)|^2. \tag{30}$$

The function  $\hat{\phi}(\xi)$  with support in the region inside this ring is a scaling function with lowpass filter  $m_0(\xi) = 2\hat{\phi}(2\xi)$  extended periodically. The highpass filter  $m_\ell(\xi)$  is the function

$$m_\ell(\xi) = \frac{2\hat{\psi}^\ell(2\xi)}{\hat{\phi}(\xi)},$$

restricted to the support of  $\hat{\psi}^\ell(2\xi)$  and extended periodically. The definition of  $m_\ell(\xi)$  is justified by the facts that

$$\text{supp } \hat{\psi}^\ell(2\xi) \subset \text{supp } \hat{\phi}(\xi)$$

and  $\hat{\phi}(\xi)$  does not vanish on the support of  $\hat{\psi}^\ell(2\xi)$ , under the additional assumption that  $\hat{\psi}^\ell(2\xi)$  goes to zero at the same rate as  $\hat{\phi}(\xi)$  goes to zero as  $\xi$  goes to the same boundary point. If

the support of  $\hat{\psi}^\ell(2\xi)$  is strictly inside the support of  $\hat{\phi}(\xi)$ , there is no need for this additional assumption. Explicitly, for a function  $f(\xi)$ , denote by  $Z(f)$  the zeros of  $f$ ; that is,

$$Z(f) := \{\xi; f(\xi) = 0\}.$$

Define

$$m_\ell(\xi) = \begin{cases} 0, & \xi \in Z(\hat{\phi}), \\ \frac{2\hat{\psi}^\ell(2\xi)}{\hat{\phi}(\xi)}, & \xi \notin Z(\hat{\phi}). \end{cases}$$

Since, by the definition of  $\hat{\phi}(\xi)$ ,

$$Z(\hat{\phi}) \subset Z(\hat{\psi}^\ell(2\cdot)),$$

the equality

$$2\hat{\psi}^\ell(2\xi) = m_\ell(\xi)\hat{\phi}(\xi)$$

holds even when  $\xi \in Z(\hat{\phi})$ . This is true independently of the value of  $m_\ell(\xi)$  for  $\xi \in Z(\hat{\phi})$ . The filters may not be continuous.

In the specific constructions of tight frames presented in this paper, the additional assumption holds and specific formulæ for the lowpass and highpass filters are given.

### 11. MULTIREOLUTION ANALYSIS FOR SMOOTH POLAR FRAME WAVELETS

Polar rings offer an arbitrary number of angular resolutions. A few sectors of annuli of the first and second dyadic rings are shown in Figure 5.

It is to be noticed that the radial interval is of the form  $[r, 2r]$ . Polar wavelets are defined by their Fourier transforms as characteristic functions over sectors of annuli. If the plane is completely covered by  $L$  nonoverlapping wedges, the  $L$  family of wavelets  $\{\psi_{j,k}^\ell\}$ , with  $\ell = 1, \dots, L$ ,  $j \in \mathbb{Z}$ , and  $k \in \mathbb{Z}^2$ , form an orthonormal basis of  $L^2(\mathbb{R}^2)$ . This basis is generated by a multiresolution analysis with scaling functions defined as in the case of box wavelets.

To have better localization in  $x$ -space, these functions are tapered with width  $2\varepsilon$  on the inside arcs, width  $4\varepsilon$  on the outside arcs, and width  $\varepsilon s$ ,  $r \leq s \leq 2r$ , on the straight edges. Provided  $\varepsilon$  is sufficiently small so that tapering overlaps are restricted to immediately adjacent regions, it will be shown below that identity (1) is satisfied. By taking a ring sufficiently close to the origin, by construction, polar rings form a Parseval frame.

The description of polar frame wavelets is considerably simplified by using the polar coordinates  $(r, \theta)$  as rectangular coordinates in the Fourier domain instead of the Cartesian coordinates  $(\xi_1, \xi_2)$ . The inverse and direct transformations are

$$\xi_1 = r \cos 2\pi\theta, \quad \xi_2 = r \sin 2\pi\theta,$$

and

$$r = \sqrt{\xi_1^2 + \xi_2^2}, \quad \theta = \frac{1}{2\pi} \arctan\left(\frac{\xi_2}{\xi_1}\right),$$

with the appropriate branches of  $\arctan$ . In the  $(r, \theta)$ -plane, the polar frame wavelets are supported in the semi-infinite strip

$$0 \leq r < \infty, \quad 0 \leq \theta \leq 1,$$

1-periodic in  $\theta$ . The strip, shown in Figure 9, is divided into rectangles with vertical sides at  $r = 2^j$ ,  $j \in \mathbb{Z}$ , and horizontal sides at

$$0 = \theta_0 < \theta_1 < \dots < \theta_\ell < \dots < \theta_L = 1.$$

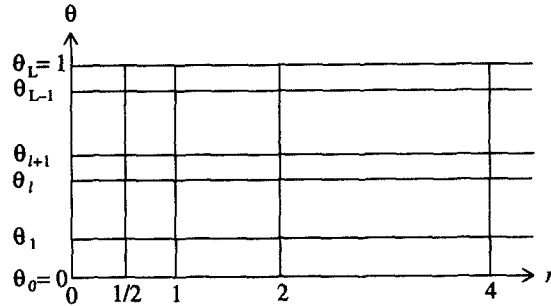


Figure 9. Strip in the  $(r, \theta)$ -plane.

The smooth functions

$$\hat{\psi}_j^\ell(r, \theta) = \hat{\psi}^\ell(2^{-j}r, \theta)$$

are easily obtained by tapering the characteristic functions of each rectangle. Tapering is done along vertical sides with transition regions of width  $2^{j+1}\varepsilon$  at  $r = 2^{j-1}$  and along horizontal sides with transition regions of width  $2\varepsilon_\ell$  with  $\varepsilon_L = \varepsilon_0$  at  $\theta = \theta_L$ . It is then clear that identity (1) is satisfied.

The smooth frame wavelets of any horizontal strip can be obtained from a multiresolution analysis. The smooth scaling function  $\hat{\phi}(r, \theta)$  is the tapered characteristic function

$$\chi_{[0,1/2] \times [0,1]}(r, \theta),$$

with transition region of width  $2\varepsilon$  along the vertical segment  $r = 1/2$ . This function corresponds to the tapered characteristic function of the disk centered at the origin with radius  $1/2$  in the  $\xi$ -space. This scaling function satisfies the identity

$$|\hat{\phi}(r, \theta)|^2 = \sum_{\ell=1}^L \sum_{j=1}^{\infty} |\hat{\psi}^\ell(2^j r, \theta)|^2$$

and the two-scale equation

$$2\hat{\phi}(2r, \theta) = m_0(r, \theta)\hat{\phi}(r, \theta), \tag{31}$$

where the lowpass filter is defined as follows. Since the function  $\hat{\phi}(2r, \theta)$  is supported on the rectangle

$$\tilde{Q} = \left[0, \frac{1}{4} + \varepsilon\right) \times [0, 1),$$

the lowpass filter  $m_0$ , defined by

$$m_0(r, \theta) = \begin{cases} 2\hat{\phi}(2r, \theta), & \text{on } \tilde{Q}, \\ 0, & \text{on } Q \setminus \tilde{Q}, \end{cases}$$

and extended  $(1 \times 1)$ -periodically, is a smooth periodic function. It follows that the Fourier transform of the scaling function  $\phi$  satisfies the two-scale equation (31).

We need only consider one wavelet, namely  $\hat{\psi}^\ell(r, \theta)$ , since the other cases are similar. The wavelet  $\hat{\psi}^\ell(r, \theta)$  satisfies the two-scale equation

$$2\hat{\psi}^\ell(2r, \theta) = m_1^\ell(r, \theta)\hat{\phi}(r, \theta), \tag{32}$$

where the highpass filter,  $m_1^\ell(r, \theta)$ , is defined as follows.

On the rectangle

$$R_1^\ell = \left\{ \frac{1}{4} - \frac{\varepsilon}{2} \leq r \leq \frac{1}{2} - \varepsilon, \theta_\ell - \varepsilon_\ell \leq \theta \leq \theta_{\ell+1} + \varepsilon_{\ell+1} \right\},$$

where  $\hat{\phi}$  is equal to 1, define

$$m_1^\ell(r, \theta) = 2\hat{\psi}(2r, \theta), \quad (r, \theta) \in R_1^\ell.$$

On the rectangular transition region

$$R_2^\ell = \left\{ \frac{1}{2} - \varepsilon \leq r \leq \frac{1}{2} + \varepsilon, \theta_\ell + \varepsilon_\ell \leq \theta \leq \theta_{\ell+1} - \varepsilon_{\ell+1} \right\},$$

where the tapering of  $\hat{\phi}(r, \theta)$  and  $\hat{\psi}^\ell(2r, \theta)$  coincide, define

$$m_1^\ell(r, \theta) = 2, \quad (r, \theta) \in R_2^\ell.$$

On the lower-right little rectangle

$$R_3^\ell = \left\{ \frac{1}{2} - \varepsilon \leq r \leq \frac{1}{2} + \varepsilon, \theta_\ell - \varepsilon_\ell \leq \theta \leq \theta_\ell + \varepsilon_\ell \right\},$$

where

$$\hat{\phi}(r, \theta) = t_r(r; \varepsilon)$$

and

$$\hat{\psi}^\ell(2r, \theta) = t_r(r; \varepsilon)t_l(\theta; \varepsilon_\ell),$$

define

$$m_1^\ell(r, \theta) = 2t_l(\theta; \varepsilon_\ell), \quad (r, \theta) \in R_3^\ell.$$

Similarly, on the upper-right little rectangle,

$$R_4^\ell = \left\{ \frac{1}{2} - \varepsilon \leq r \leq \frac{1}{2} + \varepsilon, \theta_{\ell+1} - \varepsilon_{\ell+1} \leq \theta \leq \theta_{\ell+1} + \varepsilon_{\ell+1} \right\},$$

where

$$\hat{\phi}(r, \theta) = t_r(r; \varepsilon)$$

and

$$\hat{\psi}^\ell(r, \theta) = t_r(r; \varepsilon)t_r(\theta; \varepsilon_{\ell+1}),$$

define

$$m_1^\ell(r, \theta) = 2t_r(\theta; \varepsilon_{\ell+1}), \quad (r, \theta) \in R_4^\ell.$$

One sees that in all cases

$$m_1^\ell(r, \theta) = \frac{2\hat{\psi}^\ell(2r, \theta)}{\hat{\phi}(r, \theta)}, \quad \ell = 1, 2, \dots, L,$$

over the support of  $\hat{\psi}^\ell(2r, \theta)$  and zero elsewhere in a square of sides of length 1.

## 12. A NUMERICAL IMPLEMENTATION OF THE LOCALIZATION METHOD

In this section, we apply the above theory to the restoration of finite images represented by matrices. Since the Fourier transform of a finite region gives rise to oscillations of the cardinal sine type, care must be taken in the restoration process.

The restoration process involves the following steps.

- (a) A scarred image (a) is to be restored as its original image (f).

- (b) Image (a) is Fourier transformed and filtered by multiplication with tapered characteristic functions with support far from the origin and at right angles to the singularities to be localized. This produces image (b).
- (c) The frame coefficients (13) in the Fourier domain,

$$\langle \hat{f}, \hat{\psi}_{j,k}^\ell \rangle = \langle f, \psi_{j,k}^\ell \rangle,$$

make image (c).

- (d) In view of the Plancherel theorem, image (c) is used in the  $x$  domain to obtain the wavelet frame expansion (12) of Corollary 1. This produces a thick image (d) of the singularities in image (a).
- (e) The extra width of (d), caused by the side lobes in the support of  $\psi_{j,k}^\ell$ , is narrowed to eliminate oscillations due to the cardinal sine effect when transforming functions with finite support. This is image (e).
- (f) A tuned multiple of (e) is subtracted from (a) to restore the original image (f).

Two-dimensional bell functions were produced by the Mathematica Wavelet Explorer by tapering characteristic functions over the unit square with transition widths 1/8 and 1/4 as appropriate to form the first ring of 12 functions. Tapering was done by iterating the sine function twice to get

$$b(s) = \sin\left(\frac{\pi}{2} \sin^2\left(\frac{\pi}{2} \sin^2\left(\frac{\pi}{2} s\right)\right)\right)$$

with the option `Taper -> {Trig[2], epsilon}`. It is easy to see that

$$b(s)^2 + b(1 - s)^2 = 1, \quad s \in [0, 1],$$

by noting that  $\sin((\pi/2)(1 - s)) = \cos((\pi/2)s)$  and repeated use of the identity  $\cos^2 s = 1 - \sin^2 s$ .

Six larger rings were produced by scaling the functions of the first ring. A tapered scaling function is produced from the characteristic function of the central square with sides of length 2 with transition width 1/8. The support of these functions is a square with center at the origin and sides of length 287.

These functions are evaluated in the form of tables by Mathematica and exported to MATLAB in the form of matrices

$$Q_0, Q_1^1, \dots, Q_1^{12}, \dots, Q_7^1, \dots, Q_7^{12}.$$

By construction, the  $87 \times 87$  matrix  $Q_7^2$  has lower left and upper right elements in positions (87, 201) and (1, 287). In the sequel, we shall, therefore, work with matrices of dimension  $287 \times 287$ .

A barely visible straight segment along the diagonal  $S = [(80, 80), (110, 110)]$  of a  $287 \times 287$  matrix is added to the  $256 \times 256$  matrix of the central Barbara image (a) shown in the top left part of Figure 10.

Let  $f$  be the matrix representing image (a). The discrete Fourier transform  $F$  of  $f$  is filtered by means of the top right frame,  $Q_7^2$ , of the seventh ring to recover the singularity and eliminate the smooth part of the image. We write  $k = (k_1, k_2)$ . Let the  $(m, n)$ <sup>th</sup> element of the matrix of exponentials  $E_k$  be

$$E_k(m, n) = e^{-2\pi i(m-1, n-1) \cdot (k_1, k_2)/287}. \tag{33}$$

Discretizing the scalar product (13),

$$\langle \hat{f}, \hat{\psi}_{7,k}^2 \rangle,$$

we obtain the matrix  $C = (c_k)$  of frame coefficients

$$c_k = \sum_{m,n=1}^{287} (F.*E_k.*Q_7^2)(m, n), \quad k_1 = k_2 = 1, \dots, 287, \tag{34}$$

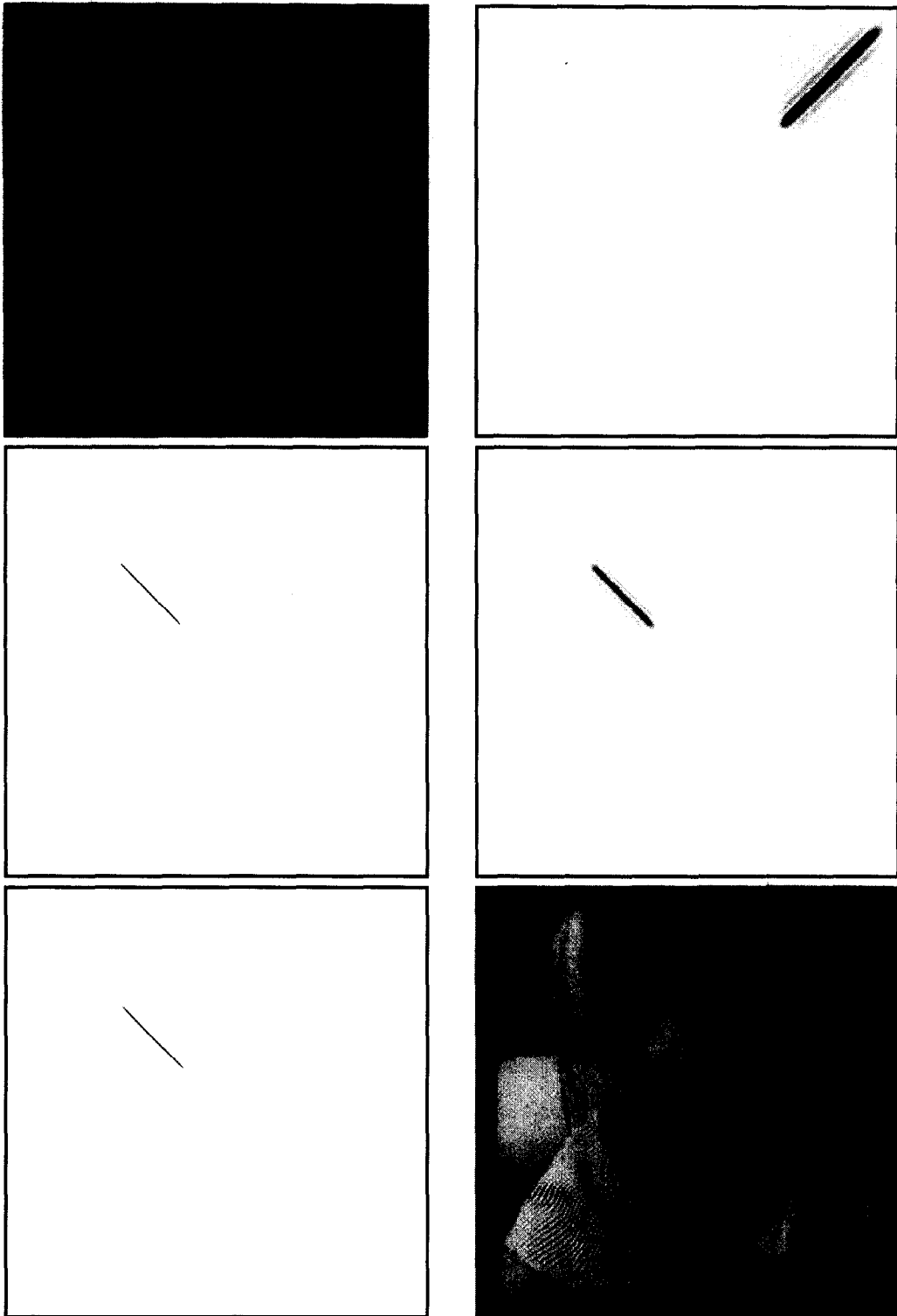


Figure 10. Top left: Image (a) of woman with scar. Top right: Image (b) of filtered Fourier transform of (a). Center left: Framed negative image (c) of frame coefficients (34) of (b). Center right: Framed negative dominantly five-pixel-thick image (d) of frame expansion of the inverse Fourier transform of (b). Bottom left: Framed negative image (e) of (d) thinned to one-pixel width. Bottom right: Restored image (f).

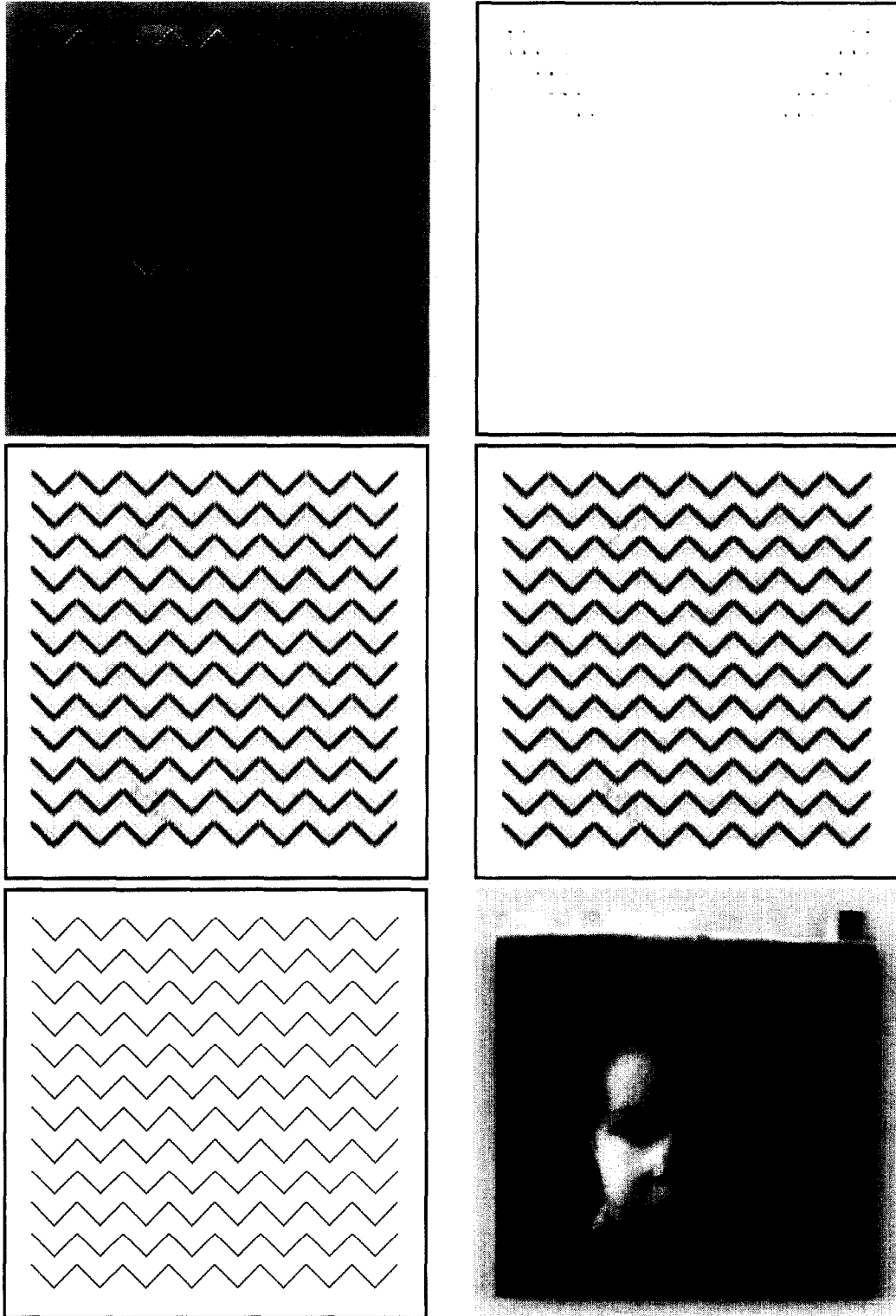


Figure 11. Top left: Image (a) of boy with grid. Top right: Image (b) of filtered Fourier transform of (a). Center left: Framed negative image (c) of frame coefficients (34) of (b). Center right: Framed negative five-pixel-thick image (d) of frame expansion of the inverse Fourier transform of (b). Bottom left: Framed negative image (e) of (d) thinned to one-pixel width. Bottom right: Restored image (f).

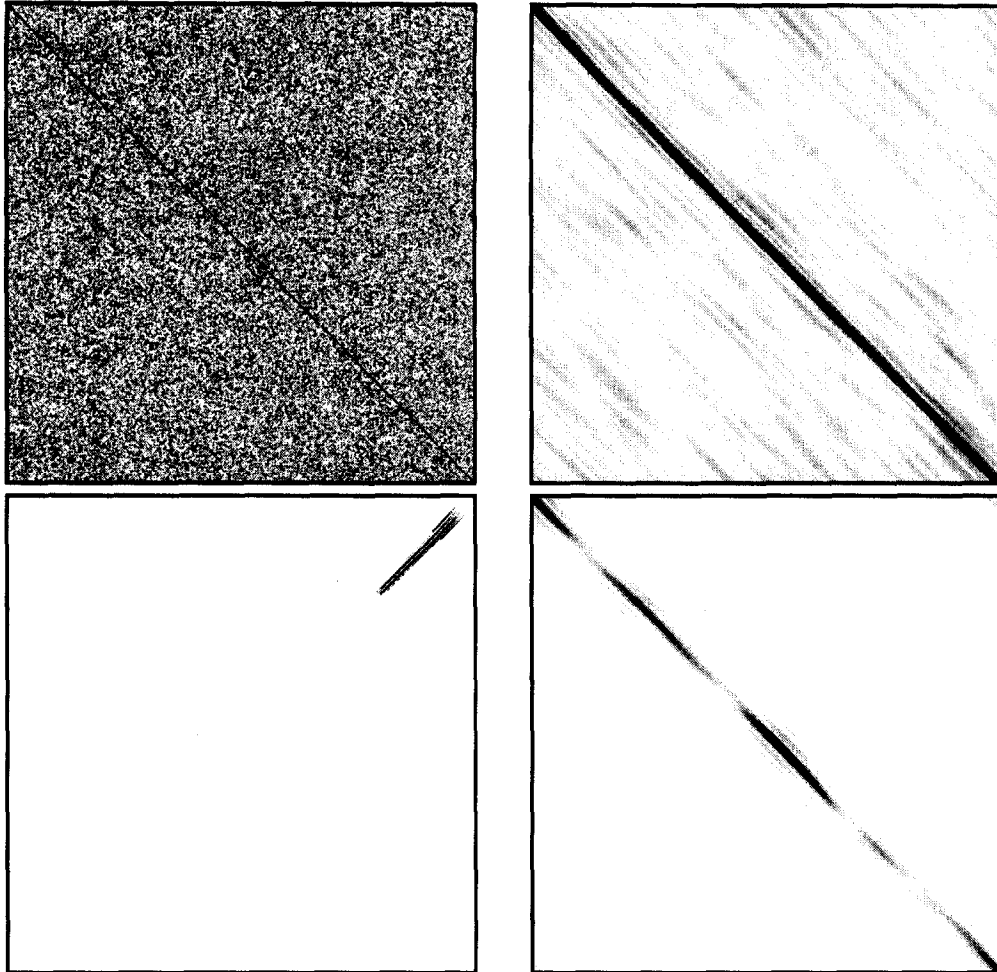


Figure 12. Top left: Framed negative image of diagonal line impulse with random noise of the same height as the line. Top right: Framed negative image of the frame coefficients of the filtered image in the Fourier domain. Bottom left and right: Framed negative image of the frame reconstruction of the filtered image in the Fourier and  $x$  domains, respectively.

where  $\cdot*$  denotes componentwise matrix multiplication. Note that  $Q_7^2$  is a real matrix. The matrix  $C$  represents image (c). The plot of the absolute value of the entries of  $C$  shown in the center left part of Figure 10 clearly indicates the dominance of the location of the singularity of the image (a).

Discretizing the partial sum (12),

$$\sum_{k_1=k_2=40}^{80} \langle \hat{f}, \hat{\psi}_{7,k}^2 \rangle \hat{\psi}_{7,k}^2(\xi),$$

we obtain the matrix  $W = (w_k)$  of the wavelet frame expansion of the discrete inverse Fourier transform of the filtered image (b). The entries of  $W$  are

$$w_k = \left( \sum_{m_1=40}^{80} c_{m_1, m_1} E_{-m_1, -m_1} * Q_7^2 \right)_k, \quad (35)$$

where summation is over the diagonal segment  $S$ . The matrix  $W$  represents image (d), shown in the center right part of Figure 10.

Since the Fourier transform of the smooth component of the image is localized mainly near the origin and the Fourier transform of the singularity consists mainly of details with high frequency, the properly modulated matrix filter  $Q_7^2$  picks up only the singularity. The use of the filter  $Q_7^8$  or both filters produces essentially the same results.

Another example consists of applying the theory developed above to remove a zigzag grid which is added to the boy image. The top left part of Figure 11 shows the boy image (a) behind a grid. The Fourier transform of (a) is filtered by two  $87 \times 87$  tapered characteristic functions in the top left and top right corners of a  $287 \times 287$  matrix in the Fourier domain at right angles to the singularities to produce image (b) in the top right part of the figure. The center left part of the figure is image (c) of the absolute values of the frame coefficients in the Fourier domain. The center right part of the figure is the frame expansion (d) of image (b) in the  $x$  domain. This frame expansion of the filtered image consists of a five-pixel-wide grid due to the finite size of the image and the width of the support of the frame wavelet functions in the  $x$  domain. This grid is thinned to the one-pixel-thick image (e) shown in the lower left part of the figure. Then a multiple of (e) is subtracted from (a) to produce the restored image (f) in the lower right part of the figure.

The frame  $\hat{\psi}_{7,k}^2(\xi)$ , with support in the top right corner in the Fourier domain, picks up the singularities across segments parallel to the main diagonal. The frame  $\hat{\psi}_{7,k}^5(\xi)$ , with support in the top left corner in the Fourier domain, picks up the singularities across segments parallel to the secondary diagonal.

The final example uses a polar frame. In the top left part of Figure 12, a random noise of height 1 has been added to a diagonal line of height 1. The Fourier transform of this image is filtered by a smooth polar frame supported on a sector of an annulus of aperture of  $0.02\pi$  radians and inner and outer radii 220 and 287, along the secondary diagonal in the upper right corner of a  $287 \times 287$  matrix in the Fourier domain. The image of the frame coefficients of the filtered image is shown in the top right part of the figure. The bottom left and right parts of the figure show the frame expansion of the filtered image in the Fourier and  $x$  domains, respectively. It is seen that there is a significant reduction in the noise.

## REFERENCES

1. J.J. Benedetto and O.M. Treiber, Wavelet frames: Multiresolution analysis and extension principles, In *Wavelet Transforms and Time-Frequency Signal Analysis*, (Edited by L. Debnath), Birkhäuser, Boston, MA, 3–36, (2001).
2. J.J. Benedetto and S. Li, The theory of multiresolution analysis frame and applications to filter banks, *Appl. Comput. Harmon. Anal.* **5**, 389–427 (1998).
3. R. Ashino, C. Heil, M. Nagase and R. Vaillancourt, Microlocal filtering with multiwavelets, *Computers Math. Applic.* **41** (1/2), 111–133 (2001).
4. R. Ashino, S.J. Desjardins, C. Heil, M. Nagase and R. Vaillancourt, Microlocal analysis, smooth frames and denoising in Fourier space, *J. of Asian Information-Science-Life* **1** (2) (July 2002).
5. S.J. Desjardins, *Image Analysis in Fourier Space*, Ph.D. Thesis, University of Ottawa, Ottawa, Ontario, (May 2002).
6. E. Hernández and G. Weiss, *A First Course on Wavelets*, CRC Press, Boca Raton, FL, (1996).
7. M. Frazier and B. Jawerth, A discrete transform and decomposition of distribution spaces, *J. Funct. Anal.* **93**, 34–170 (1990).
8. M. Frazier, B. Jawerth and G. Weiss, *Littlewood-Paley Theory and the Study of Function Spaces*, CBMS, Vol. 79, Amer. Math. Soc., Providence, RI, (1991).
9. R. Ashino, C. Heil, M. Nagase and R. Vaillancourt, Microlocal analysis and multiwavelets, In *Geometry, Analysis and Applications*, (Edited by R.S. Pathak), World Sci. Publishing, River Edge, NJ, 293–302, (2001).
10. M. Sato, Theory of hyperfunctions I, *J. Fac. Sci. Univ. Tokyo, Sec. I* **8**, 139–193 (1959).
11. L. Schwartz, *Théorie des Distributions*, 3<sup>rd</sup> edition, Hermann, Paris, (1966).
12. A. Kaneko, Microlocal analysis, In *Encyclopaedia of Mathematics*, Kluwer Academic, Dordrecht, (1997).
13. A. Kaneko, *Introduction to Hyperfunctions*, Kluwer Academic, Dordrecht, (1988).
14. A. Kaneko, *Linear Partial Differential Equations with Constant Coefficients*, (in Japanese), Iwanami, Tokyo, (1992).

15. I. Daubechies, *Ten Lectures on Wavelets*, SIAM, Philadelphia, (1992).
16. C.E. Heil and D.F. Walnut, Continuous and discrete wavelet transforms, *SIAM Rev.* **31**, 628–666 (1989).
17. R. Balan, P.G. Casazza, C. Heil and Z. Landau, Deficits and excesses of frames, *Adv. Comput. Math.* **18**, 93–116 (2003).
18. M. Frazier, G. Garrigós, K. Wang and G. Weiss, A characterization of functions that generate wavelet and related expansion, *J. Fourier Anal. Appl.* **3**, 883–906 (1997).
19. I. Daubechies, A. Grossmann and Y. Meyer, Painless nonorthogonal expansions, *J. Math. Phys.* **29**, 1271–1283 (1986).
20. S. Mallat, *A Wavelet Tour of Signal Processing*, Second Edition, Academic Press, San Diego, CA, (1999).